Organic Porosity Distribution: A Function of Aromaticity in Organic-Rich Mudrocks

by

Michael Brenden Keel

Submitted to the Department of Geology
and the Faculty of the Graduate School of The University of Kansas
in partial fulfillment of the requirements for the degree of
Master of Science

Advisory Committee:

_____
Craig P. Marshall, Co-Chair

_____
Alison Olcott Marshall, Co-Chair

_____
Eugene C. Rankey

Date Defended: 07/09/2015

The Thesis Committee for Michael Brenden Keel certifies that this is the approved version of the following thesis:

Organic Porosity Distribution: A Function of Aromaticity in Organic-Rich Mudrocks

Craig P. Marshall, Co-Chair

Alison Olcott Marshall, Co-Chair

Eugene C. Rankey

Date Approved: 07/09/2015

Abstract

Organic-rich mudrocks can have heterogeneous pore networks that affect hydrocarbon saturation and fluid flow. Organic porosity, a term used to describe pores within organic matter, contributes to a substantial proportion of the total porosity in some mudrock reservoirs. However, predicting organic pore distribution remains enigmatic. This thesis explores possible geochemical controls on organic porosity distribution and abundance with regard to organic matter type and thermal maturity using RockEval, Raman spectroscopy, focused ion beam – scanning electron microscopy (FIB-SEM), and Helium pycnometry. Comparison of RockEval and porosity data from three mudrock reservoirs were analyzed: the Ordovician Viola Group, the Cretaceous Niobrara Formation, and the Silurian "hot shale" indicates that organic porosity increases with increasing thermal maturity and decreasing hydrogen index (HI) values. Increases in both measured porosity and observed porosity (from FIB-SEM and Helium pycnometry data) with decreasing HI values (from Rock Eval data) are interpreted to result from differences in the molecular structure of Type III organic matter versus Type II organic matter. Higher organic porosity in Type III organic matter samples with low HI values is the result of increasing aromaticity, which is interpreted from RockEval and Raman spectroscopic data. Several different organic matter morphologies (lamellar and isolated macerals) coexist in certain samples, organic porosity is only located within isolated organic macerals. Based on Raman spectroscopic data, the interpreted mechanism for which increasing aromaticity develops organic pore space is the restructuring of organic macromolecules which results in the formation of aromatic islands surrounded by void space (created by the release of volatiles). With this conceptual model, reservoirs with more Type III organic matter should have a greater proportion of organic porosity, and potentially higher total porosity, than those with Type II organic matter. These

results impact organic porosity prediction and interpretation of total porosity measurements by showing that both the intrinsic cellular structure of the organic matter in a rock and thermal maturity influence the nature, amount, and distribution of organic porosity.

Acknowledgements

This research was funded by The University of Kansas General Research Fund and the Kansas Interdisciplinary Carbonates Consortium. I would like to thank Miguel Ángel Caja Rodríguez and Repsol S.A. as well as Vincent Nowaczewski and Chesapeake Energy for contributing samples and data to the project. Many thanks to my advisors, Dr. Alison Olcott Marshall and Dr. Craig P. Marshall as well as Dr. Eugene C. Rankey for serving on my committee. Thanks to my family for their constant and unwavering support, Mom, Dad, Brittany, and Evan. I would also like to thank Prem Thapa and Heather Shinogle at The University of Kansas Microscopy and Analytical Imaging Laboratory for all of their help.

Table of Contents

CHAPTER 1: INTRODUCTION 1
1.1 Preface 1
1.2 Organic Matter in Mudrocks 2
1.3 Approaches to Organic Matter Characterization 4
1.3.1 RockEval and Vitrinite Reflectance 5
1.3.2 Raman spectroscopy 7
1.4 Previous Organic Porosity Studies 8
CHAPTER 2: MATERIALS AND METHODS 8
2.1 Sampling and Geologic Context 8
2.1.1 Viola Group 9
2.1.2 Niobrara Formation 10
2.1.3 Silurian "hot shale" 11
2.3 FIB-SEM Sample Preparation 12
2.5 RockEval and TOC 13
2.6 Raman spectroscopy and Reflected Light Microscopy 13
2.7 Additional Geochemical and Petrophysical Measurements 14
CHAPTER 3: DATA AND RESULTS 14
3.1 Mineralogy and Feature Description 14
3.1.1 Viola Group 15
3.1.2 Niobrara Formation 15
3.1.3 Silurian "hot shale" 15
3.2 RockEval Data 16
3.2.1 Viola Group 16
3.2.2 Niobrara Formation 16
3.2.3 Silurian "hot shale" 16
3.3 FIB-SEM 17
3.4 Raman spectroscopy 17
3.5 Helium Porosimetry 18
CHAPTER 4: DISCUSSION 18
CHAPTER 5: CONCLUSIONS 23
REFERENCES 24
FIGURES 32

CHAPTER 1: INTRODUCTION

1.1 Preface

Increased focus on fine-grained, low permeability, unconventional mudrock reservoirs has led to a need for understanding their complex pore networks to predict hydrocarbon storage and fluid flow. Recently, researchers have described organic porosity: pore space inside organic matter within mudrocks (**Figure 1.1**) (Loucks et al., 2009; Wang and Reed, 2009; Ambrose et al., 2010; Passey et al., 2010; Schieber, 2010; Sondergeld et al., 2010; Jiang and Li, 2013). The presence of organic porosity is important because organic pores preferentially adsorb hydrocarbons to pore surfaces via weak van der Waals forces and additionally can store free hydrocarbons in pore space (Wang and Reed, 2009; Yu et al., 2014). Organic pores can have highly irregular to rounded and ellipsoidal shapes and can range in size from < 5 nm to ~1,000 nm, and many have a median size of ~100 nm (Loucks et al., 2009; Wang and Reed, 2009; Sondergeld et al., 2010). However, the controls on organic porosity distribution are not well understood. Although not all fine-grained strata contain organic porosity, it can be the only pore type present in some reservoirs. Therefore, to adequately predict porosity, permeability, and recoverable hydrocarbon reserves in fine-grained, tight formations, the controls on organic porosity distribution must be deciphered. The goal of this research is to establish the impact of initial (depositional) cellular structure of organic matter and thermal maturity on organic pore distribution and abundance in mudrocks. To address this goal, this project tests the hypothesis that the nature, amount, and distribution of organic porosity among a suite of mudrock samples from across the geologic record is controlled by differences in 1) organic matter types (explained in detail in section 1.3.1) and 2) thermal maturity. The significance of this test lies in determining

if and how thermal maturity and depositional environment (via organic matter characterization) can be used to predict organic porosity in mudrock reservoirs.

1.2 Organic Matter in Mudrocks

Geochemistry impacts organic porosity, through the processes of organic matter deposition and maturation in mudrocks. Not all mudrocks are organic-rich (a term referring to the abundance of organic matter in rock), both the deposition and the preservation of organic matter defines whether a mudrock in the geologic record is organic rich or not. In general, organic-rich mudrocks are interchangeably referred to as source rocks or potential source rocks. Organic richness is quantified by measuring the total organic carbon (TOC) in rock. The lower limit of abundance of organic carbon for source rocks is accepted to be 0.5 - 1.0 % TOC (Tissot and Welte 1978). Organic matter is produced when organisms die (leaving behind remains) or shed organic waste, such as in fecal pellets (May, 2013). Organic matter accumulation is dependent on sedimentation rate which varies with the lithology of sediment. For example, Ibach (1982) showed that TOC of different lithologies varies with the grain accumulation rates of fine-grained sediments. Slow sedimentation rates in anaerobic environments will result in higher concentrations of organic matter relative to inorganic sediment.

Preservation of organic matter is also important in maintaining high TOC in the geologic record. Increased preservation of organic matter is favored by a convergence of factors: (1) anoxia, (2) sufficiently low bioturbation, and (3) synergy between sedimentation rate and redox environment (explained below) (Killops and Killops, 2004; Loydell et al., 2013; May, 2013). Anoxia is generally accepted as one of the most important factors for preserving organic matter, because it discourages the decomposition of organic matter and influences a variety of other

factors (Killops and Killops, 2004). For example, in aerobic environments, organic matter is subject to ingestion by suspension feeders and decomposing organisms, and thus is not preserved. Oxygenated waters also encourage detritivore activity and therefore, bioturbation. Detritivores reduce the surface area of sediment particles and mix the sediment, which aids in oxygenation at the sediment-water interface and allows increased microbial degradation of organic matter (Killops and Killops, 2004; Peters et al., 2005). Anoxic conditions occur in a variety of depositional settings, including stratified water columns (which can create oxygen-poor layers) and restricted water circulation (which also depletes water bodies in oxygen, promoting increased preservation). Sedimentation rate also influences organic matter preservation and organic richness. Rapid burial can dilute the concentration of organic matter relative to inorganic sediment, but can isolate organic matter from the oxygenated water column, and thus can promote organic matter preservation (Killops and Killops, 2004; Loydell et al., 2013).

In organic-rich mudrocks, the relative proportions of molecular components in organic matter can be used to interpret source and burial history. In terms of source, different organisms produce different types of organic matter. Biologically synthesized organic macromolecules are composed of aliphatic and aromatic skeletal backbones (**Figure 1.2** and **Figure 1.3)**. Generally, terrestrial plants contribute the most to the aromatic fraction (**Figure 1.3**) of organic matter in rocks, whereas marine algae and bacteria contribute to the aliphatic fraction (**Figure 1.2**). In simplest terms, aromatic compounds are cyclic, planar molecules, which consist of carbon atoms with alternating single and double bonds; aliphatic compounds are any compound that does not display all of these characteristics (Killops and Killops, 2004). Terrestrial higher plants are composed of compounds with higher aromatic fractions (lower hydrogen content) due to greater

abundances of lignin and cellulose (common components of terrigenous plant cell walls) (**Figure 1.4**). In contrast, highly aliphatic marine planktonic sources are enriched in lipid content (**Figure 1.5**). The type, abundance, and relative deposition rates of these different organic matter sources impacts aromaticity and initial hydrogen content (Killops and Killops, 2004). Burial history also influences organic matter abundance in a rock. Temperature conditions after burial (in terms of the maximum temperature reached and the length of time at maximum temperature) also alter organic matter by thermally degrading molecules, which involves cleaving functional groups, reduction of chain length, cyclization reactions, and the development and increase of aromaticity (Killops and Killops, 2004) (**Figure 1.6).** Thermal maturation causes gradual depletion of hydrogen in the molecular structure of organic matter and the formation of bonds with higher stability (Hunt, 1996).

1.3 Approaches to Organic Matter Characterization

Since the late 1960's, advances in petroleum generation and migration theory (e.g. Welte, 1965) have resulted in an appreciation of the importance of organic geochemical concepts (such as organic matter characterization) on petroleum exploration (Tissot, 1984). Researchers recognized that the quality of hydrocarbons in reservoirs is controlled by the original organic matter and thermal evolution of the source rock (Espitalie et al., 1977). Subsequently, methodologies that examine organic matter character were developed. Bulk sample methods such as RockEval examine the overall character of organic matter in a rock, whereas microscale methods such as Raman and infrared spectroscopies examine microscale heterogeneity across a sample. Microscale methods are more suitable than bulk methods for analyzing individual organic macerals.

1.3.1 RockEval and Vitrinite Reflectance

The traditional method for obtaining geochemical information about thermal maturity and organic matter type is RockEval. RockEval analyzes the type and thermal maturity of organic matter in rock by quantifying oxygenated and hydrocarbon compounds by pyrolyzing rock in an inert atmosphere (Espitalie et al., 1977). The phase of organic matter analyzed by RockEval is kerogen, which is: the organic solvent and acid-insoluble components of organic matter (Forsman and Hunt, 1958). RockEval data can be organized and presented on a modified Van Krevelen diagram which relates atomic ratios of hydrogen, carbon, and oxygen in kerogen: H/C and O/C (**Figure 1.7**) (Tissot et al., 1987). RockEval approximates H/C and O/C ratios with values for hydrogen index (HI) and oxygen index (OI), which can then be used to identify kerogen type. This sort of kerogen type classification is a common way to characterize organic matter based on molecular composition, from which depositional environment is inferred (see below).

There are three types of kerogen: Type I kerogen implies a lacustrine algal (aliphatic) source and is oil prone, Type II kerogen is derived from a marine algal (aliphatic or aromatic) source and can be oil or gas prone, depending on the thermal evolution pathway, and Type III kerogen (aromatic) is derived from a terrigenous environment and is gas prone (Tissot, 1984). Due to the molecular structure of the compounds synthesized by different organisms, algal (aliphatic) input results in higher hydrogen content (high HI or H/C), and terrigenous input results in higher aromaticity (low HI or H/C, high OI or O/C). The thermal maturity of kerogen can be classified using vitrinite reflectance ($\%R_o$), an index based on the optical reflectance of terrigenous organic matter (Senftle and Landis, 1991). Values representing mature kerogen, associated with the oil window, are between $\%R_o$ of 0.6% and 1.35%. $\%R_o$ values below the oil

window correspond to immature kerogen, and values above this range are associated with over-mature kerogen and the gas window (Tissot et al., 1987; Senftle and Landis, 1991). The oil and gas windows represent ranges of oil and gas (hydrocarbon) generation expelled via thermocatalytic cracking of thermally mature or over-mature kerogen (Tissot, 1984; Hunt, 1996).

Another common thermal maturity index calculated using Rock-Eval is T_{max}, defined as the temperature of peak kerogen pyrolysis. T_{max} can be related to approximate $\%R_o$ values using the formula: calculated $\%R_o = (0.018*T_{max}) - 7.16$ (Peters et al., 2005). Therefore, the two indices complement each other quite well to obtain accurate thermal maturity values for mature organic matter (Tissot, 1984). However, there are various issues with these traditional approaches to source rock characterization that may lead to inaccuracies in organic porosity estimation in fine-grained rocks. RockEval is useful for analysis of bulk samples, but this method does not constrain thermal maturity or organic matter type of individual organic macerals. Differences between bulk sample and individual organic macerals can produce different predictions of thermal maturity and organic matter type, which may be significant for organic porosity estimation (which is heterogeneous on a nanometer scale) (Jaeger, 2013). For example, analysis of individual organic macerals in a sample could yield an entirely different geochemical character than that of the bulk sample. Vitrinite reflectance, which measures the intensity of reflected light from organic macerals to estimate maturation temperature, may also lead to inaccuracies because it is also a bulk sample measurement (Jaeger, 2013). Therefore, vitrinite reflectance may not be precise enough for characterizing individual organic macerals, especially for analysis of Type I and Type II kerogen; the $\%R_o$ index is based on the reflectance of hydrogen-poor, terrigenous organic matter (Senftle and Landis, 1991). Because bulk sample data do not have the precision to describe microscale geochemical heterogeneity among individual

organic macerals, organic porosity characterization should use both macroscale and microscale source rock characterization methodologies to ensure the most complete data of the organic geochemistry of a sample.

1.3.2 Raman spectroscopy

Raman spectroscopy examines the microscale heterogeneity of organic matter within a sample. Collecting Raman spectra involves impinging light on a sample, exciting the molecules in the sample, and detecting and analyzing the scattered light. The interaction of the incident light with the vibrational modes of the molecules in a sample causes a shift in frequency in some of the scattered light, and the new frequencies are referred to as Raman bands which constitute Raman spectra (Long, 1977). Raman spectroscopy is useful for determining the composition of materials. It has been used to describe the skeletal backbone of carbonaceous materials (e.g. Jehlička and Beny, 1992; Marshall et al., 2007). The thermal maturity of carbonaceous materials can also be elucidated by Raman spectroscopy (Jehlička and Beny, 1992; Roberts et al., 1995; Spotl et al., 1998; Kelemen and Fang, 2001; Jehlička et al., 2003). Raman spectra of disordered carbonaceous material (such as kerogen) is characterized by a band situated between 1580 cm^{-1} and 1620 cm^{-1}, identified as the "G" band. The G band is assigned to an in-phase, doubly degenerate C - C stretching of E_{2g2} crystal symmetry. A second band, identified as the "D" band, is situated near 1350 cm^{-1}. The D band is assigned to a A_{1g} mode which is associated with structural defects of carbonaceous material and decreasing crystallite size (Tuinstra and Koenig, 1970; Jehlička and Beny, 1992; Kelemen and Fang, 2001). Increasing thermal maturity (therefore, increasing aromaticity) results in the D band narrowing, intensifying, and shifting to relatively higher wavenumbers; the G band also narrows and intensifies for kerogen in rocks <

2.0 $\%R_o$, above which the G band changes very little (Jehlička and Beny, 1992; Spotl et al., 1998). In kerogen < 2.0 $\%R_o$, intensifying and narrowing of D and G bands occurs with increasing aromaticity (**Figure 1.8**).

1.4 Previous Organic Porosity Studies

Many researchers agree that thermal maturity is a major control on organic porosity distribution and abundance (e.g. Loucks et al., 2009; Curtis et al., 2012; Schieber et al., 2010). However, increasing thermal maturity doesn't always correlate with increasing organic porosity, and increasing TOC doesn't always correlate with increasing organic porosity. Furthermore, organic macerals with organic pores can be adjacent to organic macerals without pores (Curtis et al., 2012; Milliken et al., 2013). Because the relationships between thermal maturity and porosity, and TOC and porosity, fail to explain organic porosity distribution and abundance, researchers have suggested organic matter type as a possible control (e.g., Curtis et al., 2012). Establishing a methodology that is sufficient for examining geochemical variations between organic macerals *in situ* is critical to examining organic matter type as a control on organic porosity distribution. If organic matter type is found to be a control it is significant because porosity nature, abundance, and distribution can potentially then be associated with depositional environment (Milliken et al., 2013).

CHAPTER 2: MATERIALS AND METHODS

2.1 Sampling and Geologic Context

Samples were collected from 3 mudrock formations: 10 core samples from Lower Silurian Rhudannian stage shale (which is informally referred to as Silurian "hot shale") in northwest Africa, 7 core samples were collected from the Niobrara Formation (4 samples from 2 wells in Colorado, 3 samples from 1 well in Wyoming), 5 outcrop samples from the Viola Limestone in Southern Oklahoma (**Table 2.1**). Samples selected included potential source rocks, as determined by their fine grain size, laminations, and dark black color. Each formation sampled includes known source rocks and give the dataset a diverse range of potential lithology, organic matter, and thermal maturity.

2.1.1 Viola Group

Viola samples were collected by Chesapeake Energy from organic-rich source beds exposed in outcrops in Arbuckle Anticline, southern Oklahoma, an area on the flank of the Anadarko Basin (**Figure 2.1**). The Viola Group was deposited during the middle to late Ordovician during the marine transgression defined of part of the Tippecanoe Sloss sequence. Viola limestone can be found across the Midcontinent of the United States, but, most oil and gas production from this unit occurs in Oklahoma and Kansas. In general, Viola reservoirs are low porosity, very low permeability, and fractured carbonates (Northcutt and Johnson, 1997; Johnson, 1997). The Viola Group is a prominent source rock for the Anadarko Basin (Wang and Philp, 1997). In the Arbuckle mountains outcrops, the Viola is conformable on top of Simpson Group siliciclastics and grades conformably into the Sylvan Shale above (**Figure 2.2**) (Decker, 1933).

The Viola Group is split into three informal stratigraphic units, a lower, middle, and upper unit. The lower unit (the unit sampled for this study) consists of laminated, organic-rich lime mudstone and wackestone and is interpreted to have been deposited in an anaerobic shallow

water environment on a carbonate platform (Denison, 1997; Wang and Philp, 1997). The middle and upper units consist of echinoderm-rich skeletal grainstone and packstone and are interpreted to have been deposited in a shallow water setting, in a subtidal to intertidal environment (Dennison, 1997). Bioturbation increases up-section from the lower Viola to the upper Viola, suggesting a transition from an anaerobic setting to increasingly oxygenated waters (Wang and Philp, 1997). Intervals of the Viola Group have been silicified, and the chert has been interpreted to be the result of mobilization of silica derived from sponge spicules (Johnson, 1997). Predominant fauna found throughout the Viola Group include graptolites and trilobites, although the lower Viola contains notably fewer fossils (Decker, 1933).

Compressional tectonics began deforming the Viola Group during the Mississippian (Dennison, 1997). Uplift during the Late Mississippian and folding, thrusting, and downwarping during the Pennsylvanian caused many structural features in Oklahoma, including the Arbuckle Anticline.

2.1.2 Niobrara Formation

Three cores sampled in this study include one from the Powder River Basin and two from the Denver Basin (**Figure 2.3**). The Niobrara Formation is a marine unit deposited during the Late Cretaceous in the Western Interior Seaway, presently the Rocky Mountain Region of the United States (Longman et al., 1998). It is a self-sourcing unit of alternating chalk and marl, that ranges in thickness from 30 to 550 m (Michaels and Budd, 2014; Sonnenberg, 2011). The Late Cretaceous was a time of major marine transgression, resulting in excellent preservation potential of organic matter. The Niobrara Formation is predominantly carbonate. During sea level highstands, coccolith-dominated carbonate sediment was deposited; during lowstands,

siliciclastic input increased, resulting in deposition of marls (Sonnenberg, 2011). In general, marl intervals serve as source rocks, whereas chalk intervals are reservoirs (Sonnenberg, 2011). Samples in this study are from cores taken from the Powder River Basin and the Denver Basin (**Table 2.2** and **Figure 2.3**). Both basins are formed by the Laramide Orogeny, and represent sub-basins within the larger Western Interior Cretaceous basin (Sonnenberg, 2011). Stratigraphically, the Niobrara Formation overlies the Carlile Formation conformably in the Denver Basin, but unconformably in the Powder River Basin (**Figure 2.4**) (Taylor and Sonnenberg, 2013). The Niobrara has a conformable relationship with the overlying Pierre Shale (**Figure 2.4**) (Longman et al., 1998). It is divided into the Smoky Hill Member and the Fort Hays Limestone Member. The chalks within the Smoky Hill Member are reservoir targets and informally divided and referred to in alphabetical succession, with the stratigraphically highest chalk as "Chalk A" (Sonnenberg, 2011). The Fort Hays Limestone Member is not present in the Powder River Basin (Taylor and Sonnenberg, 2013). Across the area, Niobrara wt. % TOC ranges from 0.5-8.0. The Denver Basin Niobrara is Type II oil-prone, whereas Powder River Basin Niobrara is Type II-III oil-gas-prone (Sonnenberg, 2011).

2.1.3 Silurian "hot shale"

The Silurian "hot shale" samples collected for this study consist of early Silurian Rhuddanian stage black shale from north Africa (**Figure 2.5**), and were provided in collaboration with Repsol SA. Silurian shale units are the source rocks for approximately 90% of Paleozoic hydrocarbon reservoirs in north Africa (Luning et al, 2000). The Rhuddanian stage was a period of organic-rich "hot" (referring to high gamma-ray response well-log values) shale deposition in north Africa (**Figure 2.6**) (Luning et al., 2000). Late Ordovician sedimentation on the north African shelf was dominated by glacial sedimentation. Deglaciation, which drove a major

transgression, characterized the early Silurian, and resulted in widespread deposition of shale in Africa (Luning et al., 2000). The entire Silurian shale succession can reach over 900 m thick in some areas, however, the "hot" organic-rich shale section is generally no more than 24 m thick (Luning et al., 2000). Paleotopographic lows were major depo-centers of organic-rich shale, which likely is due to restricted water circulation and the resulting anoxic conditions that ensued (Loydell et al., 2013). Evidence of an anoxic ocean is supported by geochemistry (e.g. Armstrong et al., 2009). Post-Rhuddanian shales are organically lean. Organic matter from the Lower Silurian shale section is Type II oil-prone with little terrestrial input (Loydell et al., 2013). Terrestrial vegetation was sparse during the Silurian, therefore terrestrial Type III organic matter input should be much less than the modern (Loydell et al., 2013). However, mixed-source marine phytoplanktonic marine (notably prasinophytes) and terrigenous organic matter input has been found in Silurian strata (Romero-Sarmiento et al., 2011).

2.3 FIB-SEM Sample Preparation

Samples were cut with a rock saw to dimensions no larger than 5 cm x 3 cm x 1 cm, and Viola Group and Niobrara Formation samples were polished. Rock microtexture was then analyzed with a FEI Versa 3D Dual Beam Focused Ion Beam-Scanning Electron Microscope (FIB-SEM) at The University of Kansas Microscopy Lab. Initial scans of the sample surface were performed and features of importance were imaged using SEM. Mineral constituents were mapped using energy-dispersive spectroscopy (EDS), a feature of the FEI Versa 3D Dual Beam. EDS measurements were made on all Niobrara and Viola samples, and 6 Silurian "hot shale" samples. To examine porosity, a focused ion beam (FIB) with a Ga^+ source was used to mill all Niobrara samples, 2 Viola samples, and 6 Silurian "hot shale" samples, using the general FIB-

SEM procedure outlined in Curtis et al. (2010). A secondary electron (SE) detector imaged the rocks and Pt was deposited before milling to reduce curtaining artifacts. The creation of a flat cross-sectional surface was created by trenching around a vertical column of material on three sides with the FIB acceleration voltage at 30 kv and beam current at 65 na. From this surface, a cleaning cross-section then was milled with the FIB acceleration voltage ranging from 8 kv - 16 kv and beam current ranging 50 pa - 1 na (**Figure 2.7**). The cleaning cross-section was performed multiple times at different acceleration voltages and beam currents to achieve an ultra-flattened cross-sectional surface. Preparation of a single FIB site was dependent on the sample properties and took anywhere from 4-8 hours.

2.5 RockEval and TOC

RockEval data were collected by powdering samples with mortar and pestle followed by pyrolyzing samples in an inert atmosphere. S1 (volatile hydrocarbon content), S2 (remaining hydrocarbon generative potential), S3 (carbon dioxide content), and T_{max} were measured and recorded. Hydrogen index was calculated using the equation: HI = (100*S2) / TOC; oxygen index was calculated using the formula: OI = (100 * S3) / TOC; calculated $\%R_o$ was calculated using the formula: calc. $\%R_o = (0.018 * T_{max}) - 7.16$ (Peters et al., 2005). S2 values quantify the remaining hydrocarbons in a rock, S3 values quantify the amount of CO_2 generated. RockEval and wt. % TOC data was collected by Weatherford Labs and existing data from the USGS Core Shed in Denver. Viola Group RockEval and wt. % TOC data were collected by Chesapeake Energy. Silurian “hot shale” RockEval and wt. % TOC were collected by Repsol SA.

2.6 Raman spectroscopy and Reflected Light Microscopy

Raman analysis was performed at The University of Kansas in Dr. Craig Marshall's Raman Spectroscopy Lab at The University of Kansas. Samples were examined under reflected light microscopy to determine the morphology of organic macerals, samples containing multiple morphologies of organic matter were studied further with Raman spectroscopy. The ability to identify different organic maceral morphologies was important for comparison with porosity (from FIB-SEM). Visible Raman spectroscopy was performed at an excitation wavelength of 514.5 nm, 2400 l/mm grating, 10 s exposure time, and 1 accumulation with a Renishaw *inVia* Reflex Spectrometer. The system was calibrated with a 514.5 nm laser using an internal Si standard. Low laser power, 0.5-1.0%, was used to ensure the samples were not altered. The spectral range between 100-1800 cm^{-1} was used to collect spectra, where the D and G bands are located. Using low magnification with objectives at 5x and 20x was necessary to prevent damage to the objectives due to irregular sample surfaces.

2.7 Additional Geochemical and Petrophysical Measurements

Additional data was collected on Silurian "hot shale" samples by Repsol S.A. including: vitrinite reflectance, Helium pycnometer porosity, and x-ray diffraction.

CHAPTER 3: DATA AND RESULTS

3.1 Mineralogy and Feature Description

A diverse range of mineralogy is examined in this sample set, as shown in **Figure 3.1**. These samples provide a spectrum of rock types for analysis.

3.1.1 Viola Group

The Viola Group consists of dark black to gray laminated mudstones with extremely low clay mineral (here and below, the term "clay" implies clay mineralogy) content that range from carbonate-rich siliceous mudstones to quartz-rich carbonate mudstones (**Figure 3.1**). Quartz content in the Viola Group samples ranges from 21 - 94%, carbonate content ranges from 5 - 77%, and clay mineral content varies from 0.6 - 7%. Microscale features abundant in the Viola Group samples include calcite-filled fractures, dolomite rhombs, organic macerals, and layers containing pyrite framboids (**Figure 3.2**).

3.1.2 Niobrara Formation

Niobrara Formation samples from cores D135 and D779 consist of dark black to gray laminated clay-rich carbonate mudstone, and those from core B129 consist of mixed carbonate and clay mudstone in near equal proportions (**Figure 3.1**). Quartz content ranges from 8 - 22%, carbonate content ranges from 38 - 83%, and the clay proportion ranges from 4 - 46%. Carbonate content increases and clay mineral content decreases from south to north in Niobrara cores D779 > D135 > B129. The most common microscale features in the Niobrara samples are clay mineral laminations within carbonate matrix, pyrite framboids, organic macerals (both lamellar and isolated macerals), and pyrite-filled vugs (**Figure 3.3**).

3.1.3 Silurian "hot shale"

Silurian "hot shale" samples consist of dark gray to black laminated quartz-rich argillaceous mudstones (**Figure 3.1**). Clay mineral content ranges from 76 - 87%, quartz content

varies between 12 - 22%, and carbonate is a minor constituent ranging from 1 - 3%. Pyrite framboids are common and can be found oriented in pyrite-laminations (**Figure 3.4**).

3.2 RockEval Data

3.2.1 Viola Group

The Viola Group samples have calculated $\%R_o$ values ranging from 0.63 - 0.89, wt. %TOC values between 1.9 and 6%, and hydrogen index (HI) values > 500 mg HC/g TOC (**Figure 3.5** and **Figure 3.6**). Viola S2 values range from 11 - 37 mg HC/ g TOC. Viola samples contain Type II organic matter.

3.2.2 Niobrara Formation

Niobrara samples have calculated $\%R_o$ values between 0.58 and 0.94%, wt. %TOC ranging from 2 - 7%, and HI values varying between 89 and 548 mg HC/g TOC (**Figure 3.7** and **Figure 3.8**). HI values vary between samples in the 3 core analyzed with the following sequence: D779 < B129 < D135. Wt. %TOC was highest in D135 samples (5 - 7%), and calculated $\%R_o$ values were highest in D779 (~ 0.94). Niobrara S2 values range from 1 - 29 mg HC/g TOC. Denver Basin samples contain Type II to II-III organic matter, Powder River Basin samples contain Type III organic matter.

3.2.3 Silurian "hot shale"

Silurian "hot shale" samples have calculated $\%R_o$ values ranging from 0.67 - 0.92, wt. %TOC values between 0.86 and 5.93, and HI values from 331 - 150 mg HC/g TOC (**Figure 3.9** and **3.10**). Silurian "hot shale" S2 values range from 2 - 17 mg HC/g TOC, samples contain Type II-III to Type III organic matter.

3.3 FIB-SEM

Results from FIB-SEM cross sections show that organic porosity is not evident in all samples. In samples where organic porosity is present, it is allocated in only some of the organic matter. Even under SEM (with nanometer-scale resolution) organic porosity is not evident in Viola Group samples (**Figure 3.11**). Silurian "hot shale" samples 1-SA and 5 had no organic pores, however, organic pores are evident in samples 6 and 7 (**Figure 3.12**). Niobrara organic porosity is apparent in D779 and D135 samples. Although D779 samples contained organic porosity, some small isolated macerals without organic pores are adjacent to organic macerals with organic porosity (**Figure 3.13**). Niobrara D135 4915 (core D135, depth 4915 ft.; similar annotation used below) consisted of alternating layers of lamellar organic matter with layers of isolated organic matter (**Figure 3.14** and **Figure 3.15**). Organic porosity in D135 4915 was allocated solely in the isolated organic macerals, organic pores are not evident in the lamellar organic matter.

3.4 Raman spectroscopy

Examination of samples with reflected light microscopy assisted in the geochemical characterization of different organic maceral morphologies. Classifying organic maceral morphology was necessary for comparison with organic porosity from FIB-SEM. Most samples (Viola, Silurian "hot shale," and Niobrara) in the suite consisted of isolated organic macerals with the exception of Niobrara D135 4915 (due to relative amounts of different organic matter types, different organic matter results in different organic maceral morphology). In samples where morphological variations in organic macerals were not noted, Raman spectroscopy was not used for comparison with porosity from FIB-SEM; targeting the same individual macerals

with both Raman spectroscopy and FIB-SEM was not possible. Furthermore, no microscale geochemical variation is apparent in Viola or Silurian "hot shale" samples.

The organic matter in Niobrara D135 4915 showed compositional differences between lamellar and isolated organic macerals separated by ~5 μm (**Figure 3.14**). Raman spectra of the lamellar organic matter (**Figure 3.16**) had no bands developed, the organic matter associated with the matrix had a G band at 1608 cm^{-1} and a D band at 1358 cm^{-1}, the organic matter associated with pyrite had a G band at 1608 cm^{-1} and no D band. Raman spectroscopy shows that the lamellar organic matter have a highly aliphatic skeletal backbone, whereas the isolated organic matter surrounded by matrix has an aromatic skeletal backbone.

3.5 Helium Porosimetry

Helium porosity data was collected, in collaboration with Repsol SA, for Silurian "hot shale" samples only (for comparison with bulk geochemistry, reported in Chapter 4); no helium porosity data was collected for Niobrara and Viola samples. Silurian "hot shale" samples have a range of measured porosity from 0.2 - 2.5% (**Table 3.1**).

CHAPTER 4: DISCUSSION

In Viola, Niobrara, and Silurian "hot shale" samples, organic porosity is a result of organic matter being present in rock, but organic porosity is not present in all organic matter. In Viola samples, no organic porosity is evident (**Figure 3.11**). In Silurian "hot shale" samples, macroscale variation of organic porosity is apparent; two populations of organic matter coexist

among samples (**Figure 3.12**). In Niobrara samples, organic porosity varies on a microscale; two populations of organic matter coexist within samples (**Figure 3.14**). The Niobrara organic matter consists of either lamellar or isolated (morphologically distinct) macerals; organic pores are evident only in isolated organic macerals. Several observations (above) provide insights into how the abundance and distribution of organic porosity in Viola, Niobrara, and Silurian "hot shale" samples are related to the geochemistry of organic matter in the samples.

It is evident from observations that organic porosity can vary within (microscale) and among (macroscale) samples. In Niobrara D135 4915, for example, microscale variation in organic porosity is dependent on organic maceral morphology (only isolated organic macerals host organic pores) (**Figure 3.14** and **Figure 3.15**). However, lamellar and isolated organic matter have distinct geochemical signatures (from Raman spectroscopy). The isolated organic matter with porosity is dominated by an aromatic (molecular) skeletal backbone, lamellar organic matter which does not host porosity is dominated by an aliphatic skeletal backbone (**Figure 3.16**).

Viola and Silurian "hot shale" samples do not display the same microscale variation in organic matter morphology or organic porosity as Niobrara samples. However, the bulk geochemistry of both the Viola dataset and the Silurian "hot shale" dataset provides evidence that organic porosity is more abundant in organic matter that is dominated by aromatic organic matter. No organic porosity is apparent in Viola samples which are dominated by Type II (highly aliphatic) organic matter (**Figure 3.5** and **Figure 3.11**). Silurian "hot shale" total porosity increases with increasing thermal maturity and decreasing hydrogen content, and samples with Type III organic matter have markedly higher porosity than samples with Type II-III organic matter (**Figure 4.1** and **Figure 4.2**). The same geochemical process is responsible for increasing

thermal maturity and decreasing hydrogen in organic matter: aromatization (increasing the abundance of aromatic rings relative to aliphatic molecules) of organic molecules. Aromatization is the same process responsible for organic pore abundance and distribution in Niobrara samples (see above). Aromaticity is interpreted to be responsible for organic porosity abundance and distribution in all three sample sets (Viola, Niobrara, and Silurian "hot shale"), but is apparent at different scales.

It is evident that aromaticity controls organic pore distribution in the samples in this study. Terrigenous (Type III) organic matter contains elevated proportions of aromatic compounds, as opposed to bacterial and planktonic marine (Type II) sources, which have elevated abundances of aliphatic compounds. Therefore, given constant TOC, Type III organic matter can be expected to have a higher abundance of organic porosity than Type II organic matter because common components of terrigenous organic matter such as lignins (the constituents of vascular plants) are highly aromatic (De Leeuw and Largeau, 1993). The degree of aromaticity of organic matter can be inferred from Raman spectroscopy and HI values, which approximate the ratio of hydrogen to carbon (H/C). The H/C ratio is much lower in aromatic molecules than aliphatic molecules (e.g. benzene (C_6H_6), an aromatic molecule, has an H/C = 1; whereas hexane (C_6H_{14}), an aliphatic molecule that also has six carbon atoms, has an H/C > 2). The thermal alteration of organic matter through diagenesis, catagenesis, and finally metagenesis, involves cleaving functional groups and increasing aromaticity to form bonds with greater stability. Therefore, thermal maturation results in increasing the aromaticity of organic matter (**Figure 1.6**).

Previous studies (e.g. Loucks et al., 2009; Curtis et al., 2010; Schieber, 2010) citing increasing thermal maturity as a major control on organic porosity formation, may be explained

by the increased aromaticity with maturity (as thermal maturity causes increased aromaticity, **Figure 1.6**). Aromaticity may also explain data from Zhang et al. (2012), who show Type III organic matter has higher methane adsorption capacity than Type II or Type I organic matter. Organic pores preferentially adsorb hydrocarbons to pore surfaces, therefore, measuring methane adsorption capacity in mudrocks is an indirect method for measuring organic porosity abundance.

The interpreted mechanism by which increasing aromaticity develops organic pore space is the restructuring of organic macromolecules. Restructuring leads to the formation of aromatic islands (clusters of rings are commonly how aromatics are oriented, e.g. Mao et al., 2010) surrounded by void space created by the release of volatiles (including hydrocarbon expulsion). The void space (organic porosity) is enclosed by aromatic rings (**Figure 4.3**). Organic porosity is favored in aromatic organic matter because of the void space created during aromatization. This mechanism is not limited to geologic processes, but it is the same process noted for the formation of porosity in activated carbon (used as a molecular sieve for industrial scale applications) (e.g. Diaz-Teran et al., 2001). The process of forming porous activated carbon involves pyrolyzing lignous material (terrigenous organic matter), increasing the aromaticity of organic matter and releasing hydrocarbon gas, which leaves behind void space (Bansal et al., 1988; Diaz-Teran et al., 2001).

Organic porosity distribution and abundance could be solely controlled by organic matter abundance. Previous workers (e.g., Milliken et al., 2013) found that TOC is a stronger control on organic porosity than thermal maturity. However, Milliken et al. (2013) acknowledge that TOC displays a positive covariation with porosity in only some of the data in that study and note organic matter type could control organic pore abundance. Similar to Milliken et al. (2013),

Silurian “hot shale” samples < 5.5 wt. % TOC display a positive covariation with porosity confirming that organic matter abundance is an important control, but it alone does not explain organic porosity nature, abundance, and distribution (**Figure 4.4**).

Although the presence of organic matter is a condition necessary for the presence of organic porosity, it is not sufficient, in and of itself. High TOC does not necessarily correspond to high organic porosity (**Figure 4.4**); instead, it appears that the presence of aromatic compounds is also necessary. Aromaticity can either be elevated at the time of deposition (aromatic rings are the major molecular (structural) component of terrigenous organic matter) or it can be increased with thermal maturation. Furthermore, organic matter with an abundant aromatic fraction is more likely to form organic porosity at lower thermal maturity (than that with an abundant aliphatic fraction). Organic matter abundance and aromatic organic matter are both the necessary controls on organic porosity abundance and distribution.

These results impact organic porosity prediction and interpretation of total porosity measurements by showing that the intrinsic cellular structure of the organic matter in rock influences the nature, amount, and distribution of organic porosity. The significance if this finding is that (1) rocks with predominantly Type III or (2) thermally mature (aromatized) organic matter are prone to higher organic porosity abundance. The areal distribution of these two attributes (above) can be used, in part, to determine the most economic zones of a mudrock reservoir, based on the principle that areas with higher porosity can accommodate an increased abundance of hydrocarbons.

CHAPTER 5: CONCLUSIONS

The major findings of this research are (1) Given equal TOC, mudrocks with greater abundance of Type III organic matter than of Type II-III mixed source organic matter or Type II organic matter have greater organic porosity; (2) Increasing aromaticity is interpreted to be the cause of this phenomenon; (3) Organic pore abundance increases with thermal maturity, which is also due to increasing aromaticity; (4) Organic pores begin to form at the onset of maturity (% R_o ~0.6). Therefore, this study establishes that organic matter type and thermal maturity are controls on organic porosity nature, abundance, and distribution.

REFERENCES

Ambrose, R.J., Hartman, R.C., Diaz-Campos, M., Akkutlu, I.Y., Sondergeld, C.H., 2010, New pore-scale considerations for shale gas in-place calculations, paper presented during SPE Unconventional Gas Conference held in Pittsburgh, Pennsylvania, February 23-25.

Armstrong, H.A., Abbott, G.D., Turner, B.R., Makhlouf, I.M., Muhammad, A.B., Pedentchouk, N., Peters, H., 2009, Black shale deposition in an upper Ordovician-Silurian permanently stratified peri-glacial basin, southern Jordan: Paleogeography, Paleoclimatology, Paleoecology, v. 273, no. 3-4, p. 368-377

Bansal, R.C., Donnet, J.B., Stoeckli, F., 1988, Active carbon: Marcel Dekker, New York, p. 237.

Curtis, M.E., Ambrose, R.J., Energy, D., Sondergeld, C.H., Rai, C.S., 2010, Structural characterization of gas shales on the micro- and nano-scales, paper presented during Canadian Unconventional Resources & International Petroleum Conference held in Calgary, Alberta, Canada, October 19-21.

Curtis, M., Cardott, B., Sondergeld, C., Rai, C., 2012, The development of organic porosity in the Woodford Shale related to thermal maturity, paper presented during SPE Annual Technical Conference and Exhibition held in San Antonio, Texas, October 8-10.

Decker, C.E., 1933, Viola Limestone, Primarily of Arbuckle and Wichita Mountains regions, Oklahoma: AAPG Bulletin, v. 17, no. 12, p. 1405-1435.

De Leeuw, J.W., Largeau C., 1993, Chapter 2: A review of macromolecular organic compounds that comprise living organisms and their role in kerogen, coal, and petroleum formation, *in*

Organic Geochemistry Principles and Applications (eds. Engel, M.H., and Macko, S.A.), Plenum Press, New York, New York, p. 23-72.

Denison, R.E., 1997, Contrasting sedimentation inside and outside the southern Oklahoma aulacogen during the middle and late Ordovician, *in* Simpson and Viola Groups in the Southern Midcontinent (ed. Johnson, K.S.), 1994 symposium: Oklahoma Geological Survey Circular 99, p. 39-47.

Diaz-Teran, J., Nevskaia, D.M., Lopez-Peinado, A.J., Jerez, A., 2001, Porosity and adsorption properties of activated charcoal: Colloids and Surfaces A, v. 187-188, p. 167-175.

Espitalie, J., Madec, M., Tissot, B., 1977, Source rock characterization method for petroleum exploration, paper presented during the Offshore Technology Conference in Houston, Texas, May 2-5.

Forsman, J.P., Hunt, J.M., 1958, Insoluble organic matter (kerogen) in sedimentary rocks of marine origin: Geochimica et Cosmochimica Acta, v. 15, no. 3, p. 170–182.

Hunt, J.M., 1996, Petroleum Geochemistry and Geology, W.H. Freeman, New York, New York, p. 743.

Ibach, L.E.J., 1982, Relationship between sedimentation rate and total organic carbon content in ancient marine sediments: AAPG Bulletin, v. 66, no. 2, p. 170-188.

Jaeger, H., 2013, Optical kerogen analysis- a new workflow in unconventional shale play analysis, paper presented during Unconventional Resources Technology Conference held in Denver, Colorado, August 12-14.

Jehlicka, J., Beny, C., 1992, Application of raman micro-spectrometry in the study of structural changes in Precambrian kerogens during regional metamorphism: Organic Geochemistry, v. 18, no. 2, p. 211–213.

Jehlicka, J., Urban, O.U., Pokorny, J., 2003, Raman spectroscopy of carbon and solid bitumens in sedimentary and metamorphic rocks: Spectrochimica Acta Part A, v. 59, no. 10, p. 2341-2352.

Jiang, Z., Li, Q., 2013, Reservoir characteristics and evaluation methods of tight lacustrine carbonates: example from Shulu Sag in Bohai Bay, China, paper presented during Unconventional Resources Technology Conference held in Denver, Colorado, August 12-14.

Kelemen, S.R., Fang, H.L., 2001, Maturity trends in raman spectra from kerogen and coal: Energy & Fuels, v. 15, no. 3, p. 653-658.

Killops, S., Killops, V., 2004, Introduction to organic geochemistry, Blackwell Publishing, Malden, Massachussetts, p. 408.

Long, D.A., 1977, Raman spectroscopy, *in* The Characterization of Chemical Purity: Organic Compounds (ed. Staveley, L.A.K.), McGraw-Hill, New York City, New York, p. 149-162.

Longman, M.W., Luneau, B.A., Landon, S.M., 1998, Nature and distribution of Niobrara lithologies in the Cretaceous western interior seaway of the Rocky Mountain region: The Mountain Geologist, v. 35, no. 4, p. 137-170.

Loucks, R.G., Reed, R.M., Ruppel, S.C., Jarvie, D.M., 2009, Morphology, genesis, and distribution of nanometer-scale pores in siliceous mudstones of the Mississippian Barnett Shale: Journal of Sedimentary Research, v. 79, no. 12, p. 848–861.

Loucks, R.G., Reed, R.M., Ruppel, S.C., Hammes, U., 2012, Spectrum of pore types and networks in mudrocks and a descriptive classification for matrix-related mudrock pores: AAPG Bulletin, v. 96, no. 6, p. 1071–1098.

Loydell, D.K., Butcher, A., Fryda, J., 2013, The middle Rhuddanian (lower Silurian) 'hot' shale of north Africa and Arabia: an atypical hydrocarbon source rock: Paleogeography, Paleoclimatology, Paleoecology, v. 386, p. 233-256.

Luning, S., Loydell, D.K., Sutcliffe, O., Ait Salem, A., Zanella, E., Craig, J., Harper, D.A.T., 2000, Silurian - Lower Devonian black shales in Morocco: which are the organically richest horizions?: Journal of Petroleum Geology, v. 23, no. 7, p. 293-311.

Marshall, C.P., Love, G.D., Snape, C.E., Hill, A.C., Allwood, A.C., Walter, M.R., Van Kranendonk, M.J., Bowden, S.A., Sylva, S.P., Summons, R.E., 2007, Structural characterization of kerogen in 3.4 Ga archaean cherts from the Pilbara Craton, Western Australia: Precambrian Research, v. 155, no. 1-2, p. 1–23.

Mao, J., Fang, X., Lan, Y., Schimmelmann, A., Mastalerz, M., Xu, L., Schmidt-Rohr, K., 2010, Chemical and nanometer-scale structure of kerogen and its change during thermal maturation investigated by advanced solid-state ^{13}C NMR spectroscopy: Geochimica et Cosmochimica Acta, v. 74, no. 7, p. 2110-2127.

May, J.A., 2013, The sedimentology of mudrocks: organics, organisms, and occasional occurences, paper presented during the Unconventional Resources Technology Conference held in Denver, Colorado, August 12-14.

Michaels, J., Budd, D.A., 2014, Pore systems of the B-Chalk zone in the Niobrara Formation, Denver-Julesburg Basin, Colorado, paper presented during the Unconventional Resources Technology Conference held in Denver, Colorado, August 25-27.

Milliken, K.L., Rudnicki, M., Awwiller, D.N., Zhang, T., 2013, Organic matter-hosted pore system, Marcellus Formation (Devonian), Pennsylvania: AAPG Bulletin, v. 97, no. 2, p. 177–200.

Northcutt, R.A., Johnson K.S., 1997, Major Simpson and Viola oil and gas reservoirs in Oklahoma, *in* Simpson and Viola Groups in the Southern Midcontinent (ed. Johnson, K.S.), 1994 symposium: Oklahoma Geological Survey Circular 99, p. 38-57.

Passey, Q.R., Bohacs, K.M., Esch, W.L., Klimentidis, R., Sinha, S., 2010, From oil-prone source rock to gas-producing shale reservoir – geologic and petrophysical characterization of unconventional shale-gas reservoirs, paper presented during CPS/SPE International Oil & Gas Conference and Exhibition held in Beijing, China, June 8-10.

Peters, K.E., M.R. Cassa, 1994, Applied source rock geochemistry, *in* The Petroleum System; from Source to Trap: AAPG Memoir 60 (eds. Magoon, L.B., and Dow, W.G.), p. 93-120.

Peters, K.E, Walters, C.C., Moldowan, J.M., 2005, The Biomarker Guide: Biomarkers and Isotopes in the Environment and Human History, Cambridge University Press, Cambridge, UK, p. 471.

Roberts, S., Tricker, P.M., Marshall, J.E.A., 1995, Raman spectroscopy of chitinozoans as a maturation indicator: Organic Geochemistry, v. 23, no. 3, p. 223-228.

Romero-Sarmiento, M.-F., Riboulleau, A., Vecoli, M., Versteegh, G. J.-M., 2011, Aliphatic and aromatic biomarkers from Gondwanan sediments of late Ordovician to early Devonian age: an early terrestrialization approach: Organic Geochemistry, v. 42, no. 6, p. 605-617.

Schieber, J., 2010, Common themes in the formation and preservation of intrinsic porosity in shales and mudstones - illustrated with examples across the Phanerozoic, paper presented during SPE Unconventional Gas Conference held in Pittsburgh, Pennsylvania, February 23-25.

Senftle, J.T., Landis, C.R., 1991, Vitrinite reflectance as a tool to assess thermal maturity, *in* Source and Migration Processes and Evaluation Techniques (Merrill, R.K. ed.), American Association of Petroleum Geologists, p. 119–125.

Sondergeld, C.H., Ambrose, R.J., Rai, C.S., 2010, Micro-structural studies of gas shales, paper presented during SPE Unconventional Gas Conference held in Pittsburgh, Pennsylvania, February 23-25.

Sonnenberg, S.A., 2011, The Niobrara petroleum system: a new resource play in the Rocky Mountain region, *in* Revisiting and Revitalizing the Niobrara in the Central Rockies (eds.

Estes-Jackson J.E., and Anderson, D.S.), Rocky Mountain Association of Geologists, p. 13-32.

Spotl, C., Housekneckt, D.W., Jaques, R.C., 1998, Kerogen maturation and incipient graphitization of hydrocarbon source rocks in the Arkoma Basin, Oklahoma and Arkansas: a combined petrographic and raman spectrometric study: Organic Geochemistry, v. 28, no. 9, p. 535-542.

Taylor, J., Sonnenberg, S.A., 2013, Reservoir characterization of the Niobrara Formation, southern Powder River Basin, Wyoming: The Mountain Geologist, v. 51, no. 1, p. 83-108.

Tissot, B.P., 1984, Recent advances in petroleum geochemistry applied to hydrocarbon exploration: AAPG Bulletin, v. 68, no. 5, p. 545–563.

Tissot, B.P., Pelet, R., Ungerer, P.H., 1987, Thermal history of sedimentary basins, maturation indices, and kinetics of oil and gas generation: AAPG Bulletin, v. 71, no. 12, p. 1445–1466.

Tissot, B.P., Welte, D.H., 1978, Petroleum Formation and Occurrence, New York, Springer Verlag, p. 539.

Tuinstra, F., Koenig, J.L., 1970, Raman spectrum of graphite: The Journal of Chemical Physics, v. 53, no. 3, p. 1126-1130.

Vieler, A., Wilhelm, C., Goss, R., Suß, R., Schiller, J., 2007, The lipid composition of the unicellular green alga *Chlamydomanas reinhardtii* and the diatom *Cyclotella meneghiniana* investigated by MALDI-TOF MS and TLC: Chemistry and Physics of Lipids, v. 150, p.143-155.

Wang, H.D., Philp, R.P., 1997, Geochemical study of potential source rocks and crude oils in the Anadarko Basin, Oklahoma: AAPG Bulletin, v. 81, no. 2, p. 249–275.

Wang, F.P., Reed, R.M., 2009, Pore networks and fluid flow in gas shales, paper presented during SPE Annual Technical Conference and Exhibition held in New Orleans, Louisiana, October 4-7.

Welte, D.H., 1965, Relation between petroleum and source rocks: AAPG Bulletin, v. 49, no. 12, p. 2246-2268.

Yu, W., Sepehrnoori, K., Patzek, T.W., 2014, Evaluation of gas adsorption in Marcellus Shale, paper presented during the SPE Annual Technical Conference and Exhibition held in Amsterdam, The Netherlands, October 27-29.

Zhang, T., Ellis, G.S., Ruppel S.C., Milliken, K., Yang, R., 2012, Effect of organic-matter type and thermal maturity on methane adsorption in shale-gas systems: Organic Geochemistry, v. 47, p. 120-131.

FIGURES

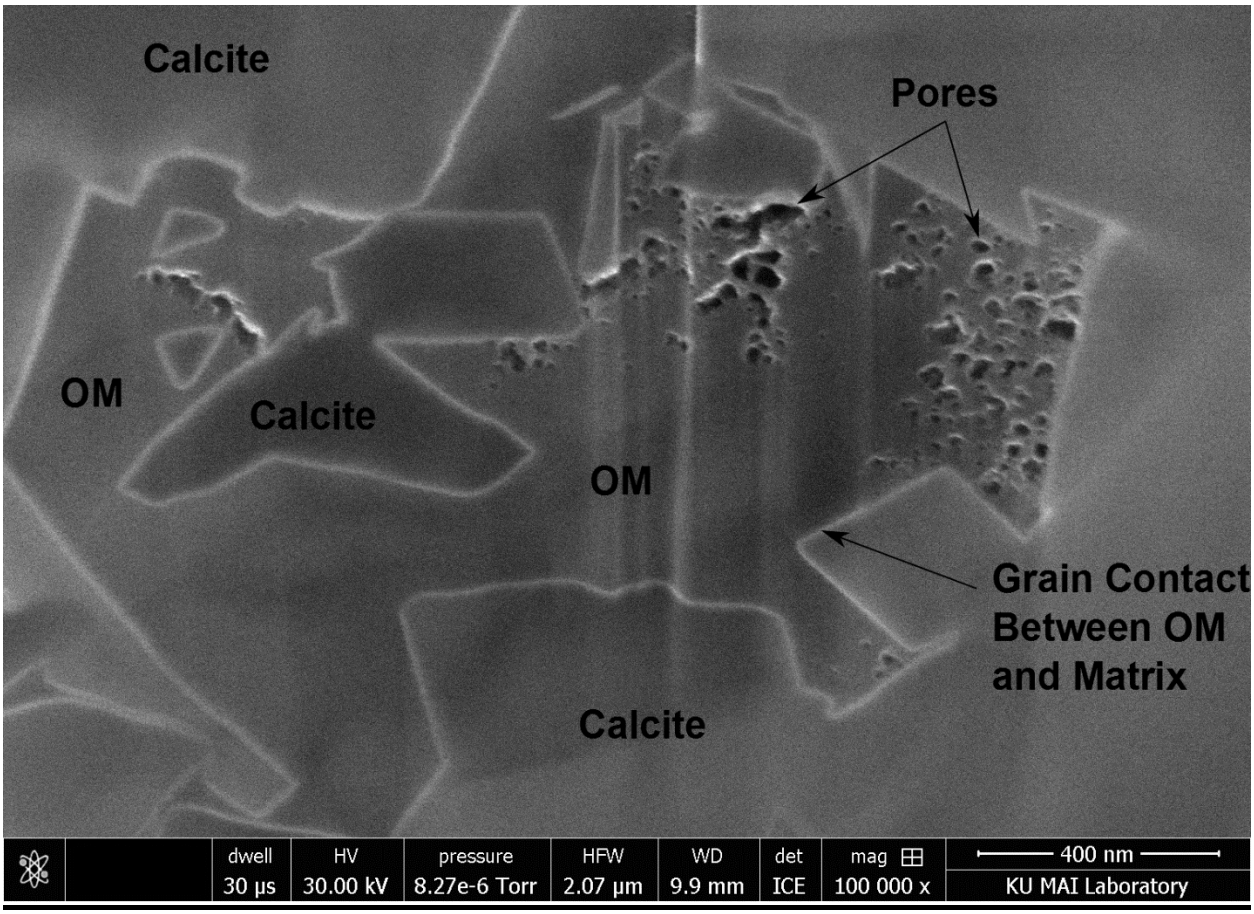

Figure 1.1- 2D SEM image from the Niobrara Formation showing organic porosity. Dark grey polygonal organic maceral bounded by a sharp white line (indicating the grain boundary) surrounded by slightly lighter grey calcite matrix. Dark black to grey elliptical and irregular shapes within the organic maceral (also bounded by sharp white lines) are organic pores.

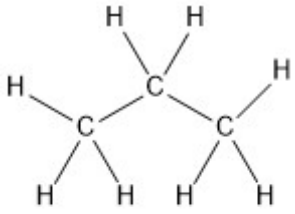

Figure 1.2- Representation of a type aliphatic molecule: Explicitly labelled skeletal notation (upper) and normal skeletal notation (lower) drawings of an aliphatic propane molecule (C_3H_8).

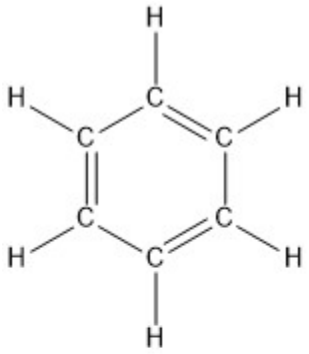

Figure 1.3- Representation of a type aromatic molecule: Explicitly labelled skeletal notation (upper) and normal skeletal notation (lower) drawings of an aromatic benzene molecule (C_6H_6). Notice this molecular arrangement is comprised of a ring of alternating C=C (double bonds) and C-C (single bonds) bonds.

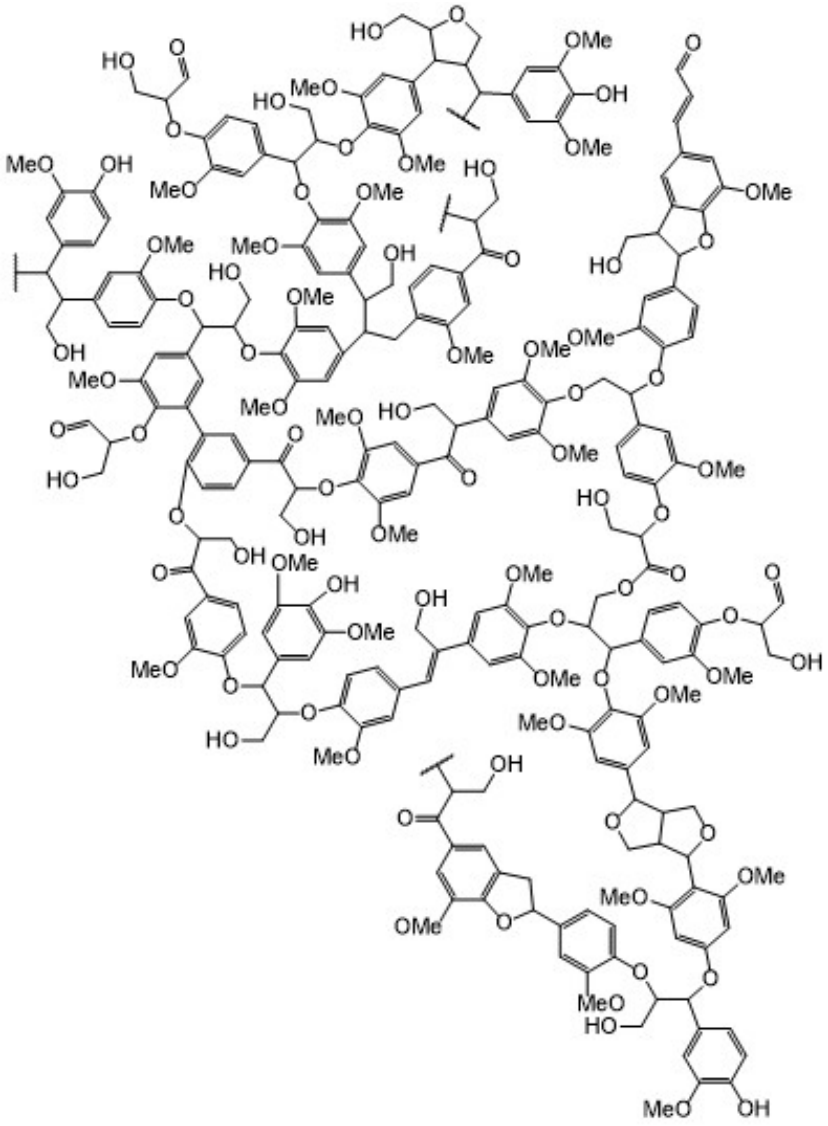

Figure 1.4- Illustration of the molecular structure of lignin. Notice the abundance of aromatic rings and uncommon short-chained aliphatic molecules (modified from Killops and Killops, 2004).

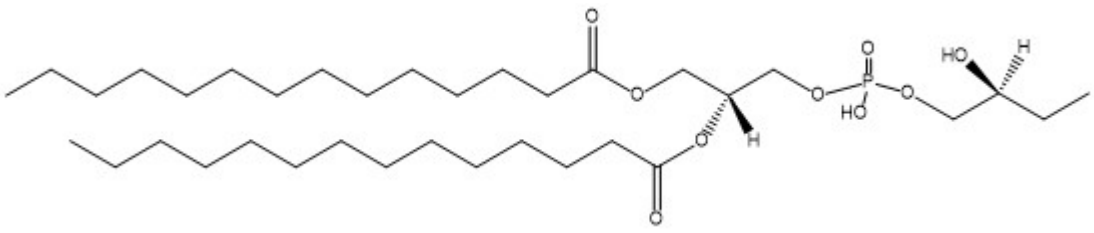

Figure 1.5- Illustration of phosphatidylglycerol, a common lipid found in green algae. Lipids are a major contributor to the organic matter derived from algal sources (modified from Vieler et al., 2007).

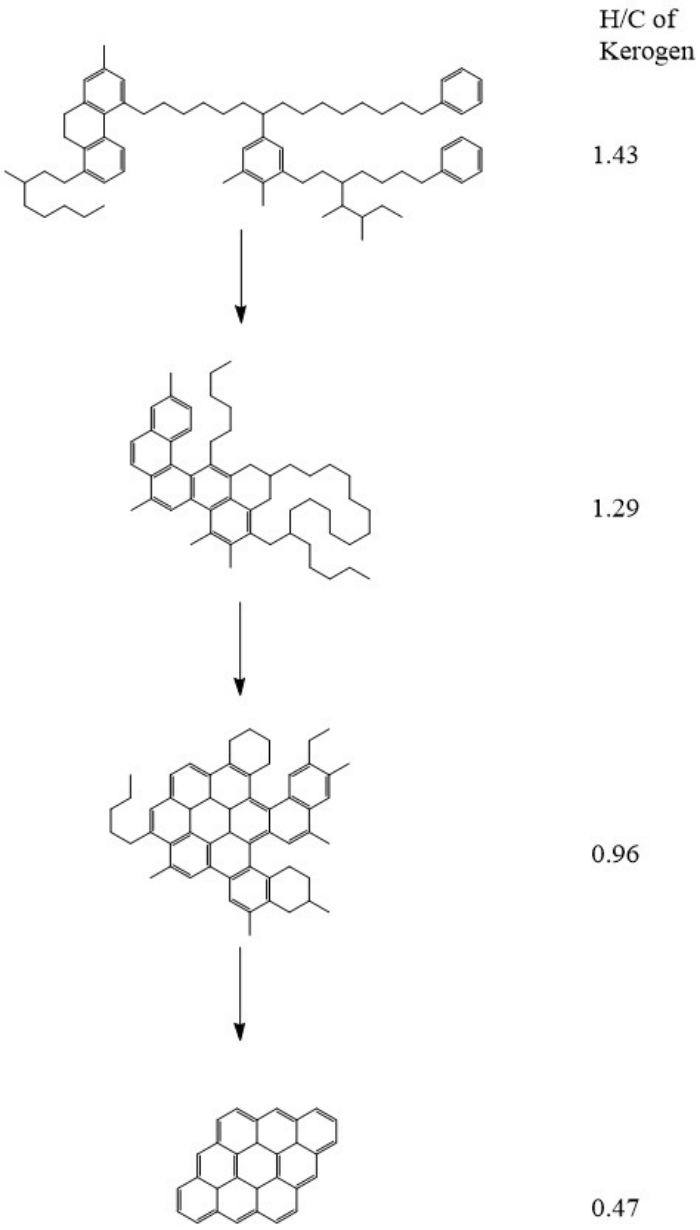

Figure 1.6- Schematic diagram representing structural changes with thermal alteration of organic matter. The ratio of Hydrogen to Carbon (H/C) decreases as thermal maturity increases. Thermal maturation increases the aromatic fraction of molecules until aromatic sheets are all that remain of the original organic matter (modified from Hunt, 1996).

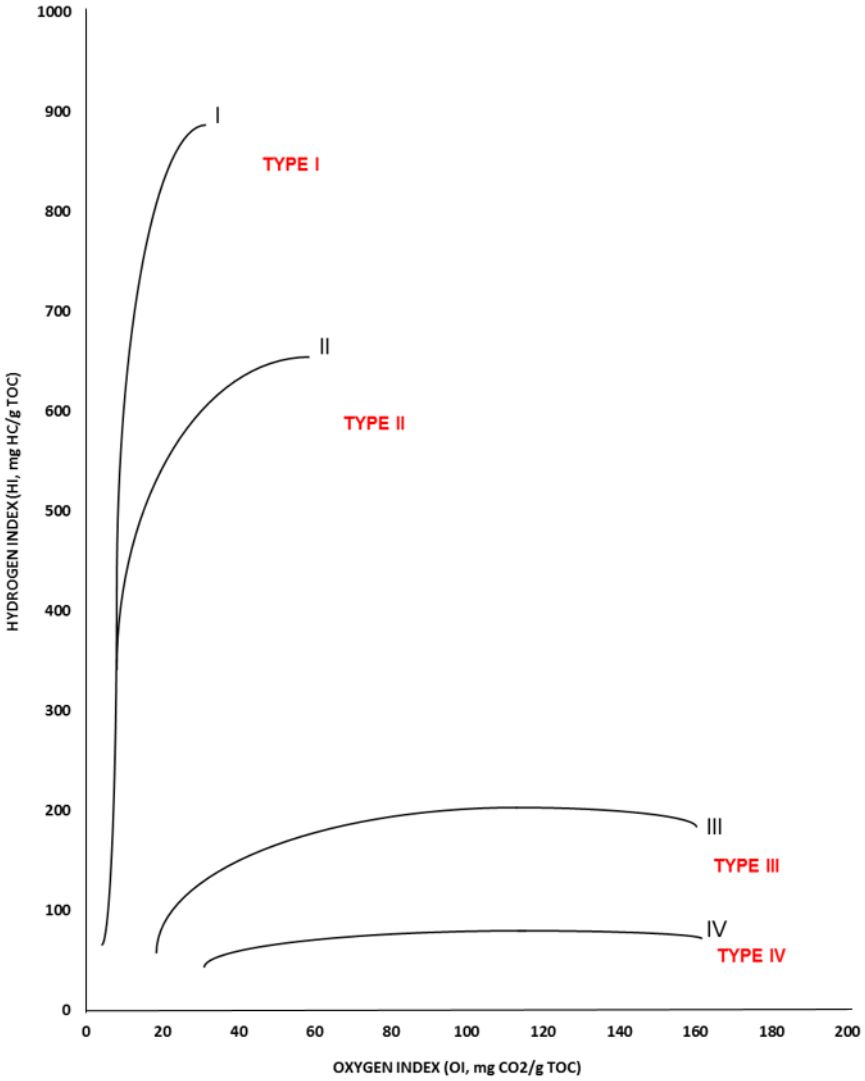

Figure 1.7- Modified Van Krevelen diagram illustrating how organic matter type can be determined.

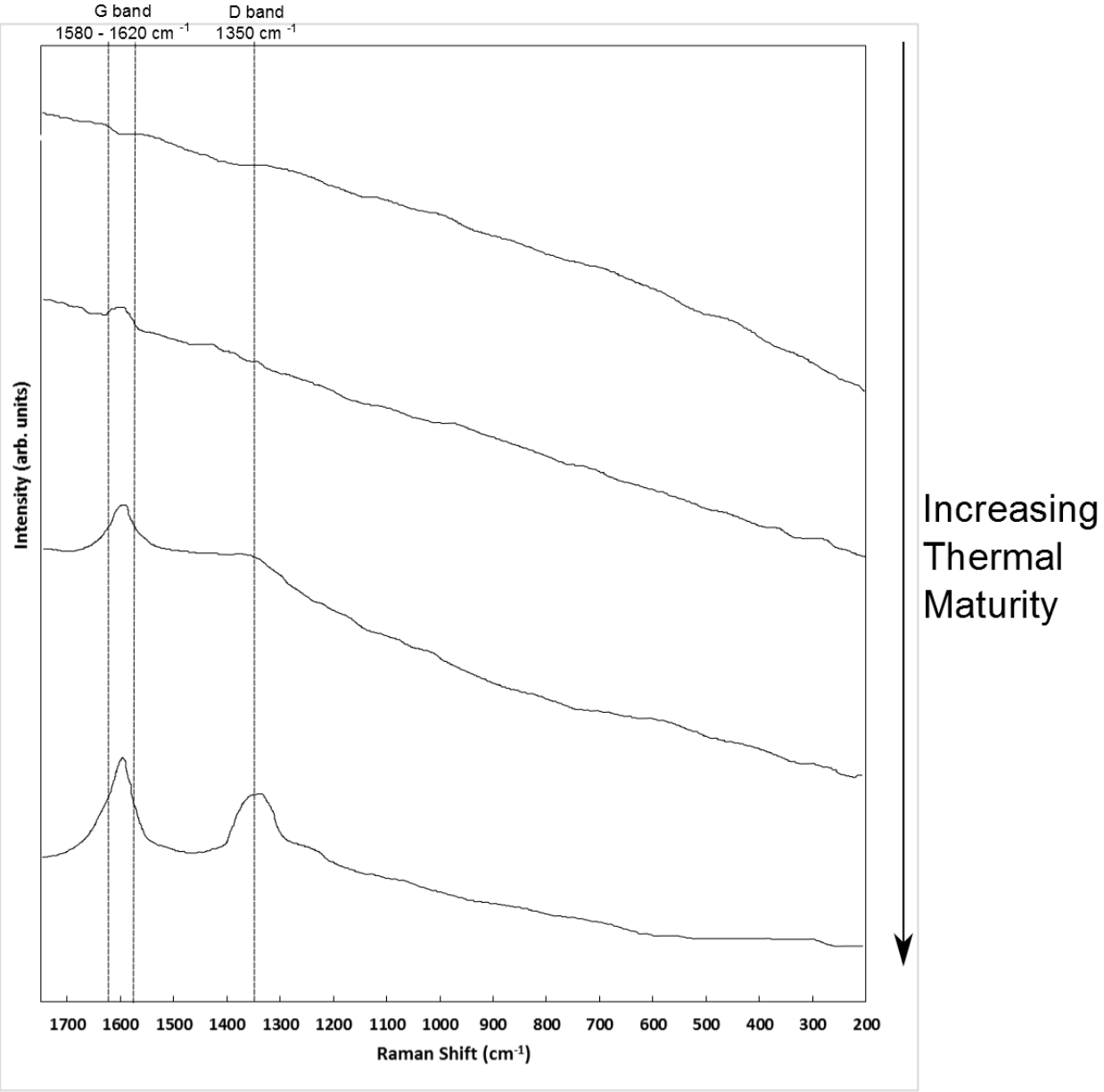

Figure 1.8- Idealized Raman spectra of kerogen (for kerogen < 2.0 %Ro). With increasing thermal maturity, aromaticity increases and D and G bands intensify and narrow.

Formation	Sample	Locale	Type
Silurian Hot Shale	1-SA	N. Africa	core
Silurian Hot Shale	2	N. Africa	core
Silurian Hot Shale	3	N. Africa	core
Silurian Hot Shale	4	N. Africa	core

Silurian Hot Shale	5	N. Africa	core
Silurian Hot Shale	6	N. Africa	core
Silurian Hot Shale	7	N. Africa	core
Silurian Hot Shale	8	N. Africa	core
Silurian Hot Shale	9	N. Africa	core
Silurian Hot Shale	10	N. Africa	core
Niobrara	B129 2927	Denver Basin	core
Niobrara	B129 3085	Denver Basin	core
Niobrara	D135 4912	Denver Basin	core
Niobrara	D135 4915	Denver Basin	core
Niobrara	D779 10388.5	Powder River Basin	core
Niobrara	D779 10390	Powder River Basin	core
Niobrara	D779 10399	Powder River Basin	core
Viola	6B	Arbuckle Mountains	outcrop
Viola	9A	Arbuckle Mountains	outcrop
Viola	9B	Arbuckle Mountains	outcrop
Viola	4B-A	Arbuckle Mountains	outcrop
Viola	10A	Arbuckle Mountains	outcrop

Table 2.1- Core and outcrop samples used in this study.

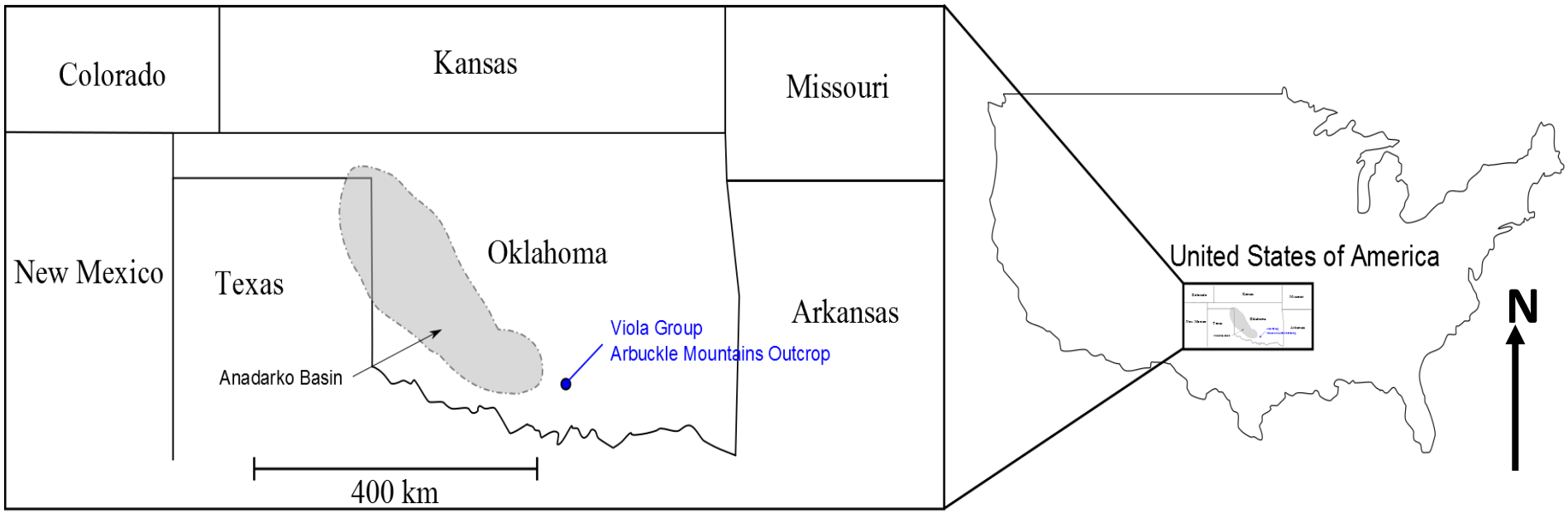

Figure 2.1- Map showing location of Arbuckle Mountains outcrops, Oklahoma, USA. Note that this area is adjacent to the Anadarko Basin, in which the Viola Group is a source rock.

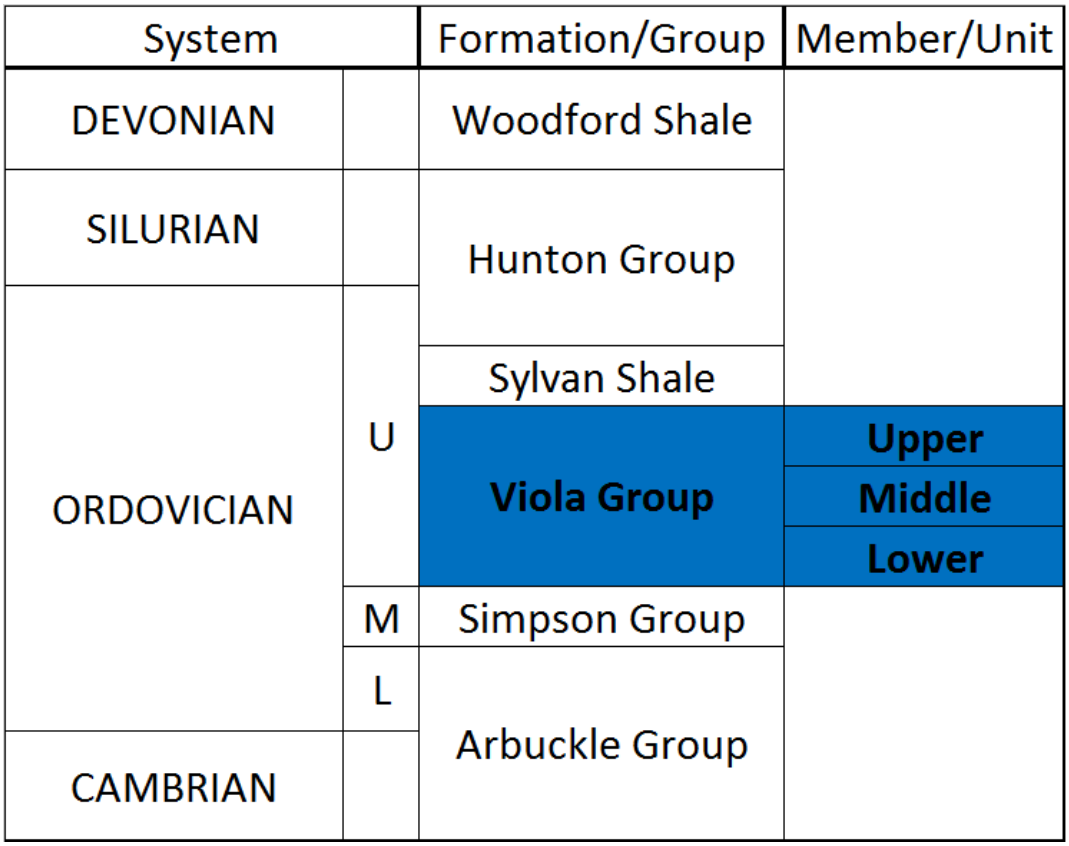

Figure 2.2- Stratigraphic column of south-central Oklahoma, highlighting the Viola Group. Modified from Wang and Philp (1997).

Well Name	Basin	Location	Core Label
Bass Phillippi Baker 15-42	Denver Basin	23N 66W 15	D135
JT Federal 1-12	Powder River Basin	32N 69W 12	D779
Berthoud State # 3	Denver Basin	4N 69W 16	B129

Table 2.2- Niobrara wells and their corresponding core labels. Niobrara samples are referred to by their core label followed by depth sampled (e.g. D135 4915).

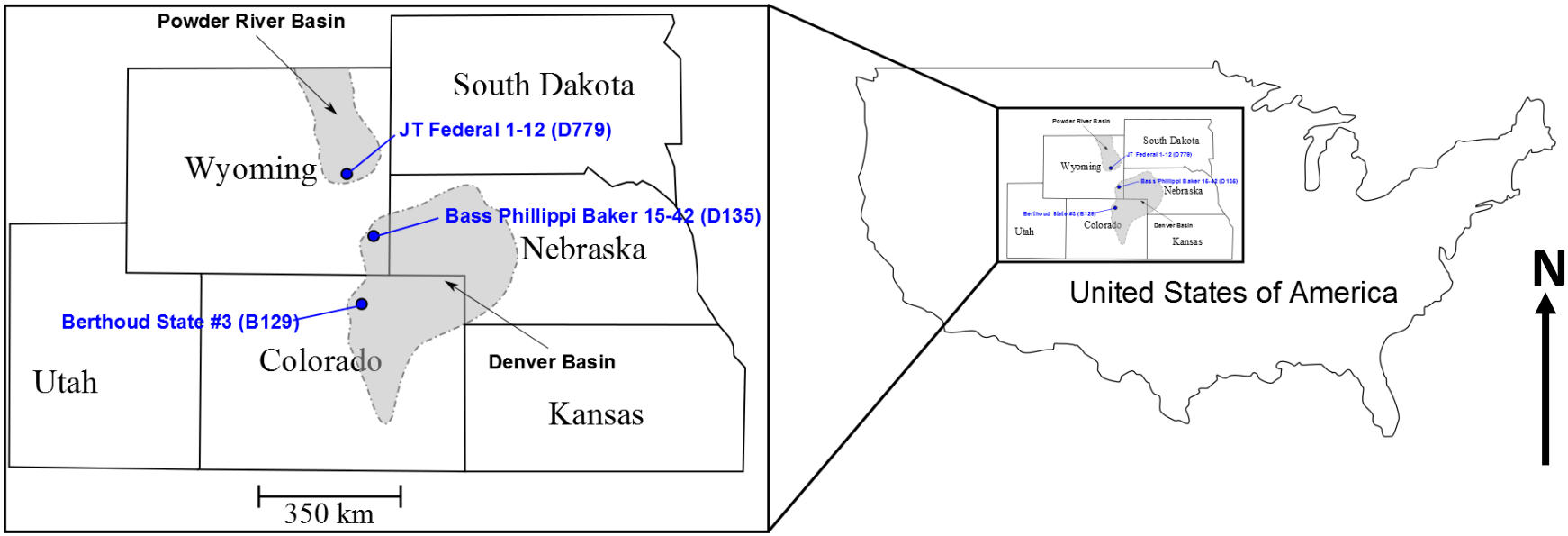

Figure 2.3- Map illustrating the locations of the 3 Niobrara cores used in this study.

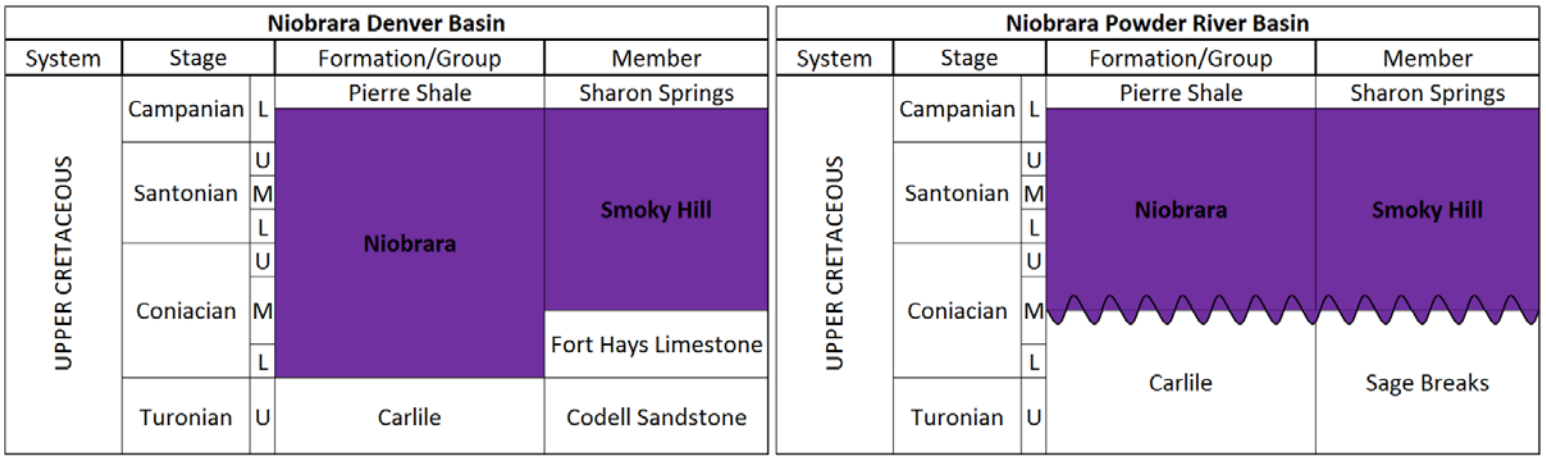

Figure 2.4- Stratigraphic column of the Denver and Powder River basins. Modified from Sonnenberg (2011) and Taylor and Sonnenberg (2013).

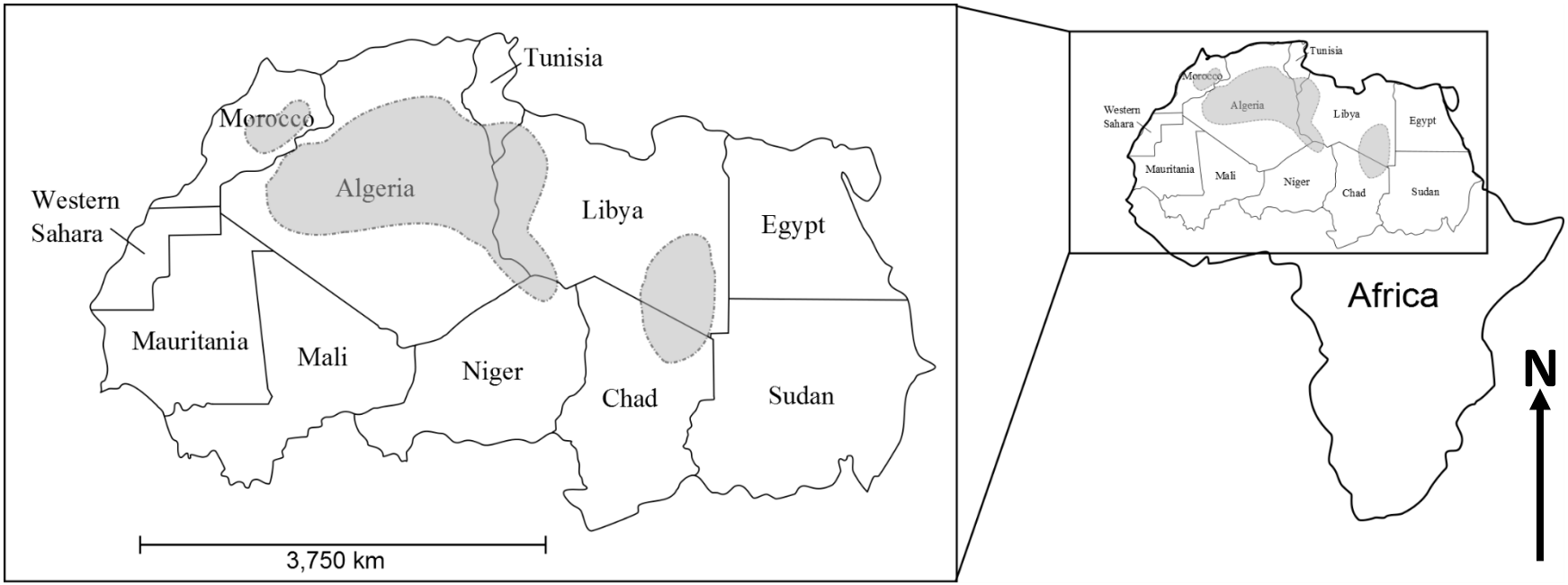

Figure 2.5- Areal distribution of Silurian "hot shale", outlining major basins. Modified from Luning et al. (2000).

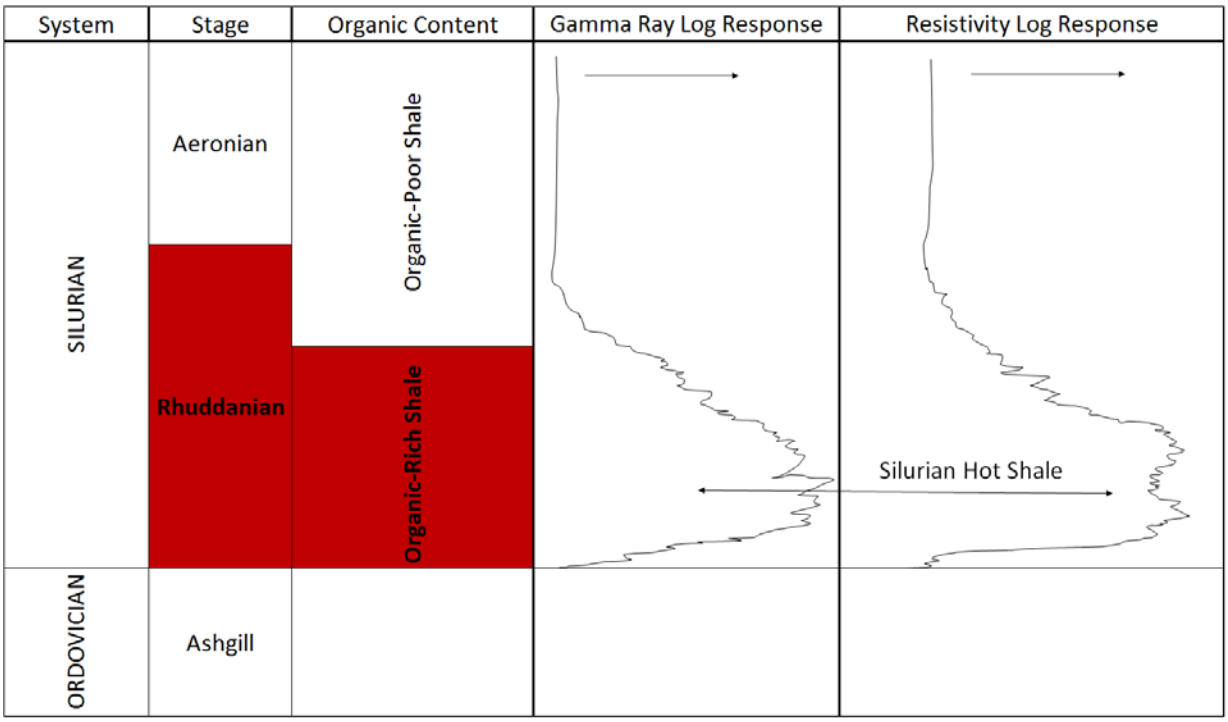

Figure 2.6- Stratigraphic column and schematic log response showing the Silurian "hot shale" of north Africa. Modified from Luning et al. (2000).

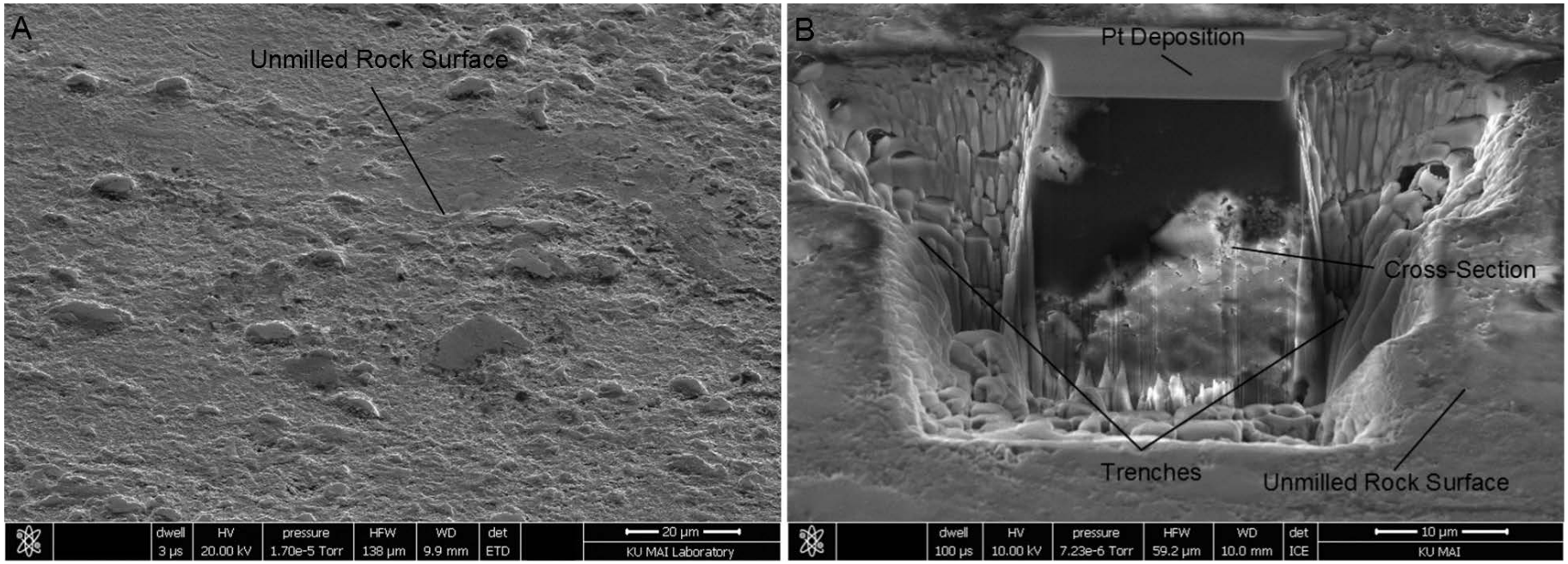

Figure 2.7- (A) Unmilled rock area, and (B) FIB-SEM cross-sectioned site with Pt deposition site and trenches. Notice the differences in rock microtexture between the two. For this sample, porosity is only evident with FIB-SEM preparation.

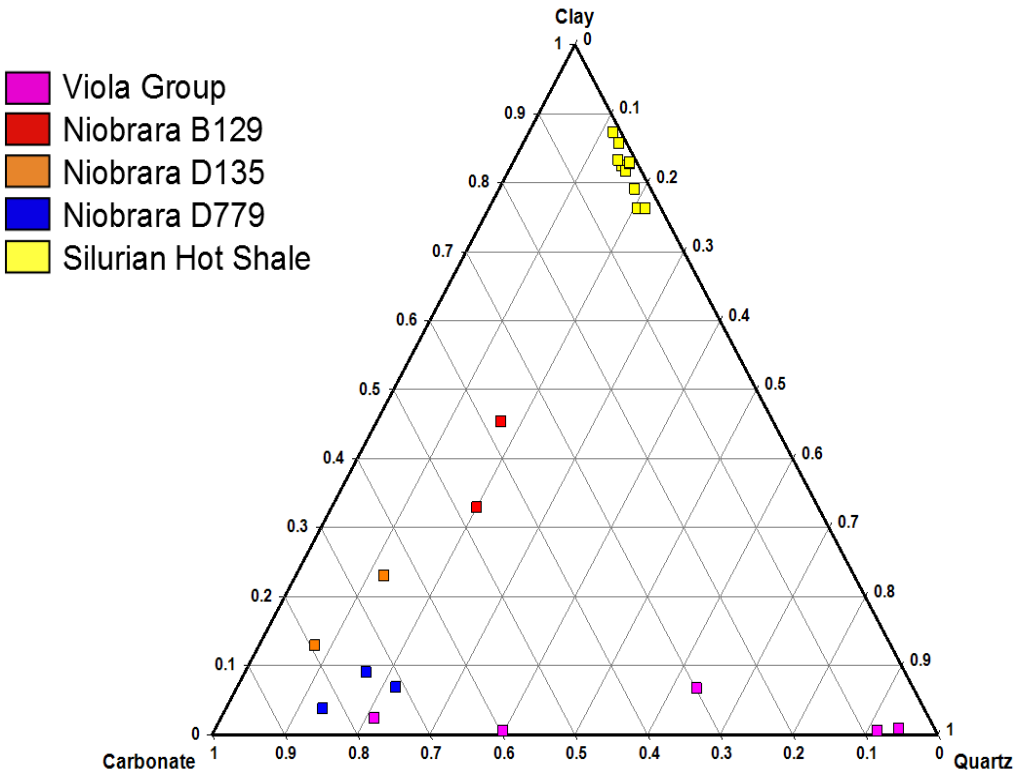

Figure 3.1- Ternary diagram showing the mineralogy of samples in the dataset based on carbonate, quartz, and clay endmembers. EDX and XRD data were used for mineralogy classification.

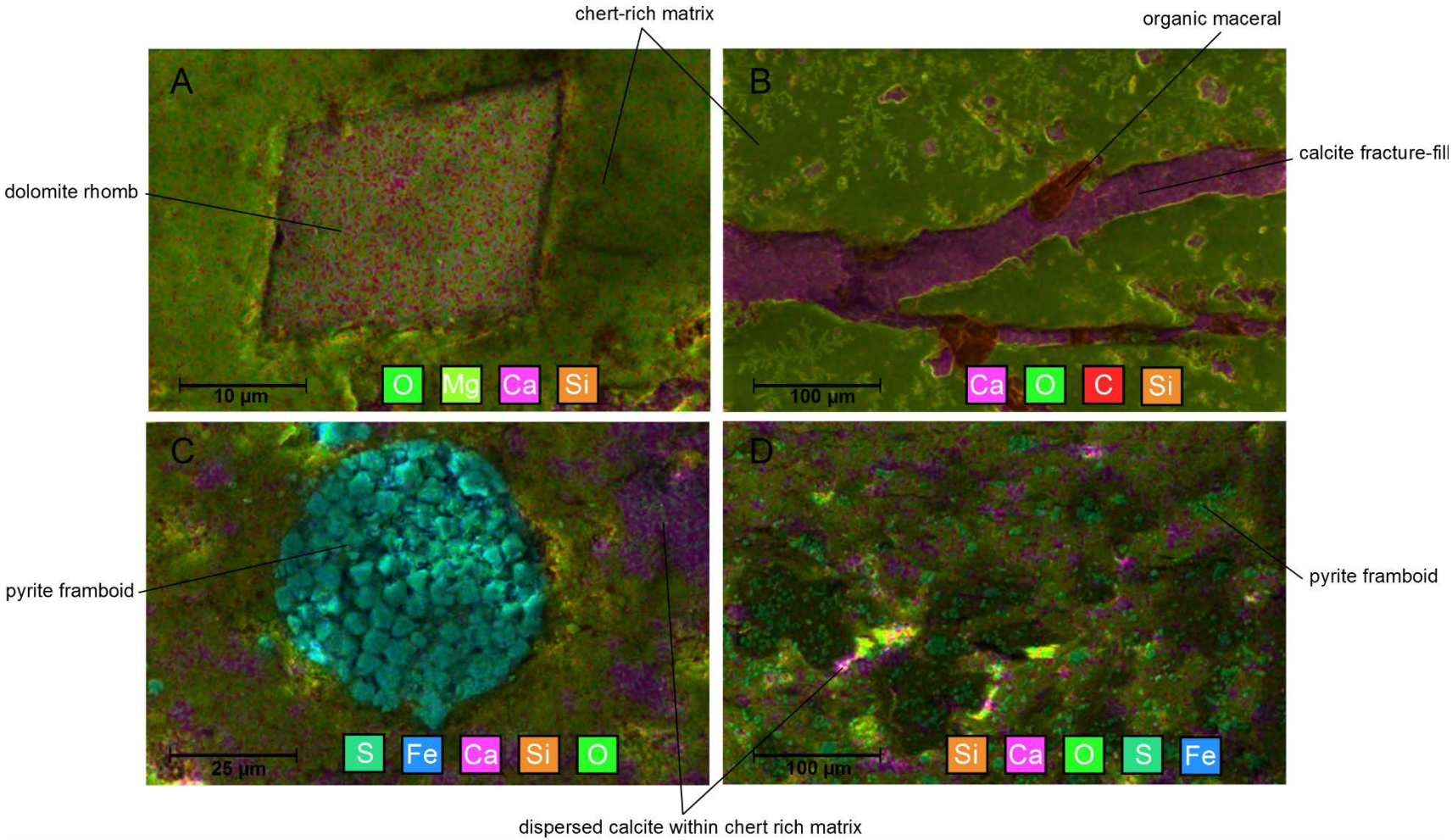

Figure 3.2- Viola Group EDX maps, which illustrate compositional differences (as distinct colors) within and among samples (A) dolomite rhomb (denoted by high Mg) surrounded by a chert matrix (B) calcite-filled fracture cutting through the chert matrix. Note the organic macerals, denoted by red color (C) pyrite framboid, a common feature in Viola samples (D) pyrite-rich zone (blue-green features) surrounded by a chert-rich matrix with some dispersed carbonate.

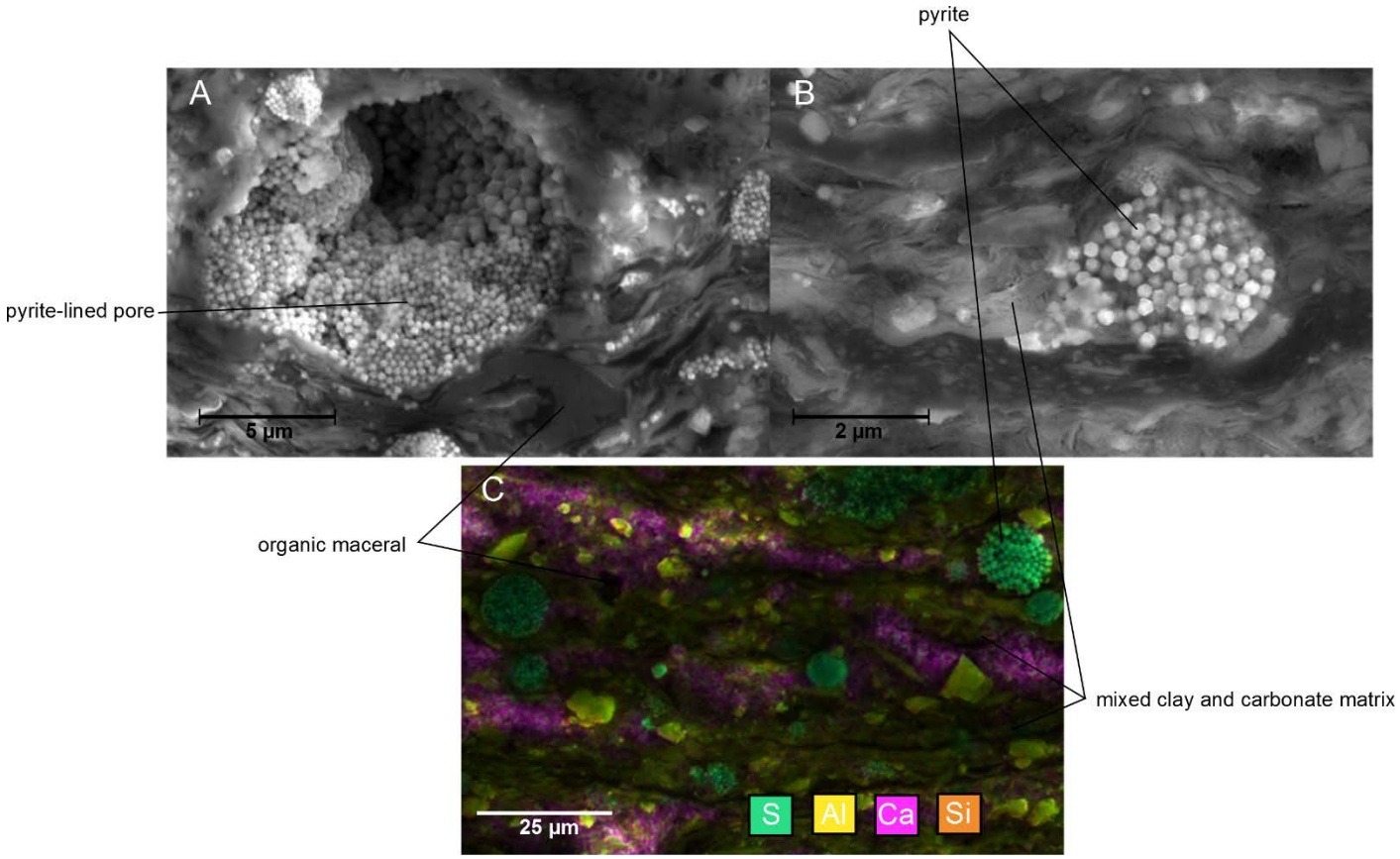

Figure 3.3- SEM images and EDX map from Niobrara samples (A) pyrite lined pore surrounded by interspersed clay, carbonate, pyrite, and organic macerals (B) pyrite framboid surrounded by clay and carbonate (C) EDX map showing the colored distribution on matrix constituents.

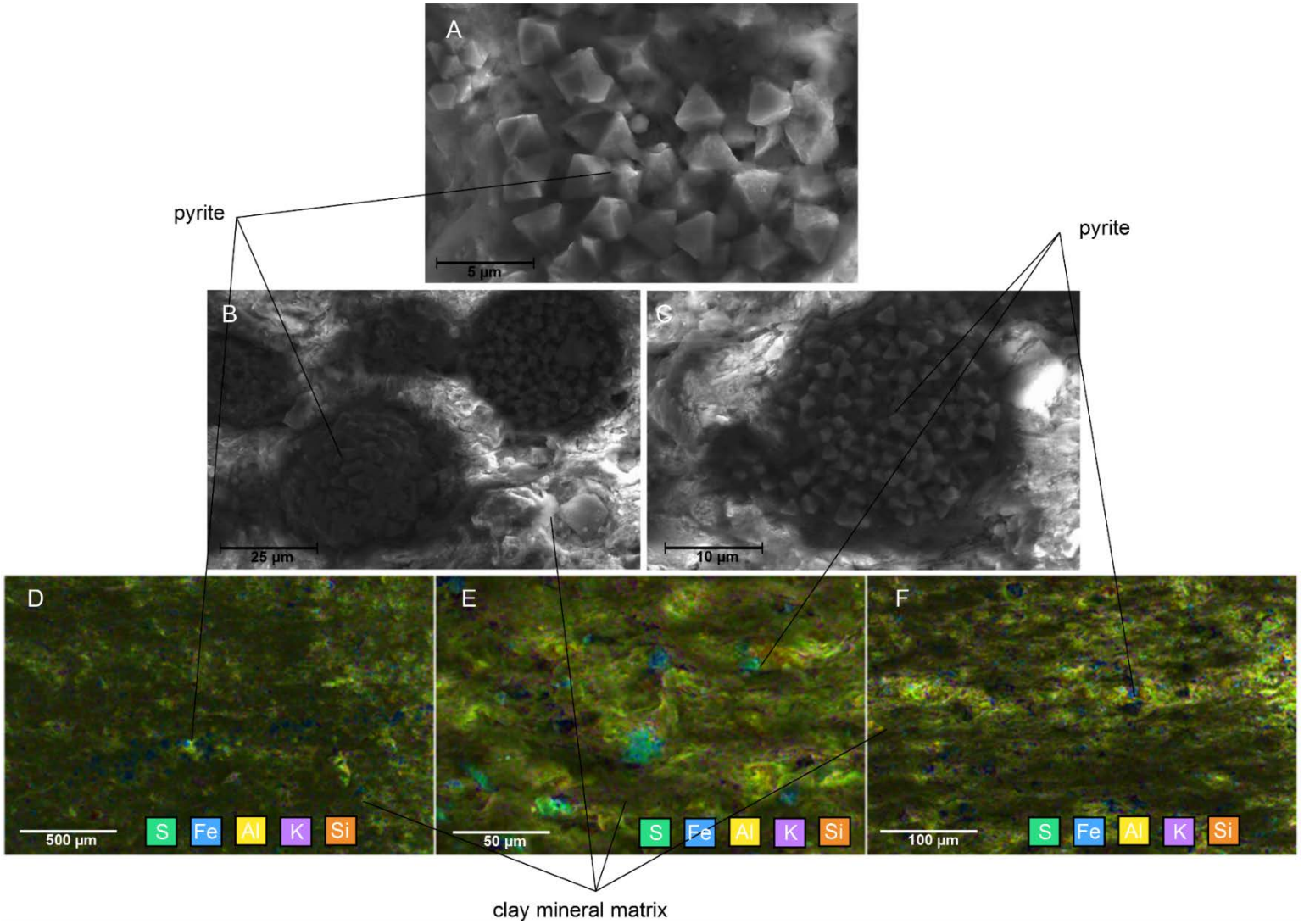

Figure 3.4- Silurian "hot shale" SEM images and EDX maps (A) octahedral pyrite crystals (B) pyrite framboids surrounded by clay matrix (C) pyrite framboid, notice void spaces between individual crystals (D) EDX map showing a zone of pyrite enrichment surrounded by clay matrix (E) dispersed pyrite framboids surrounded by clay matrix (F) zone of pyrite framboids, note that they are randomly dispersed.

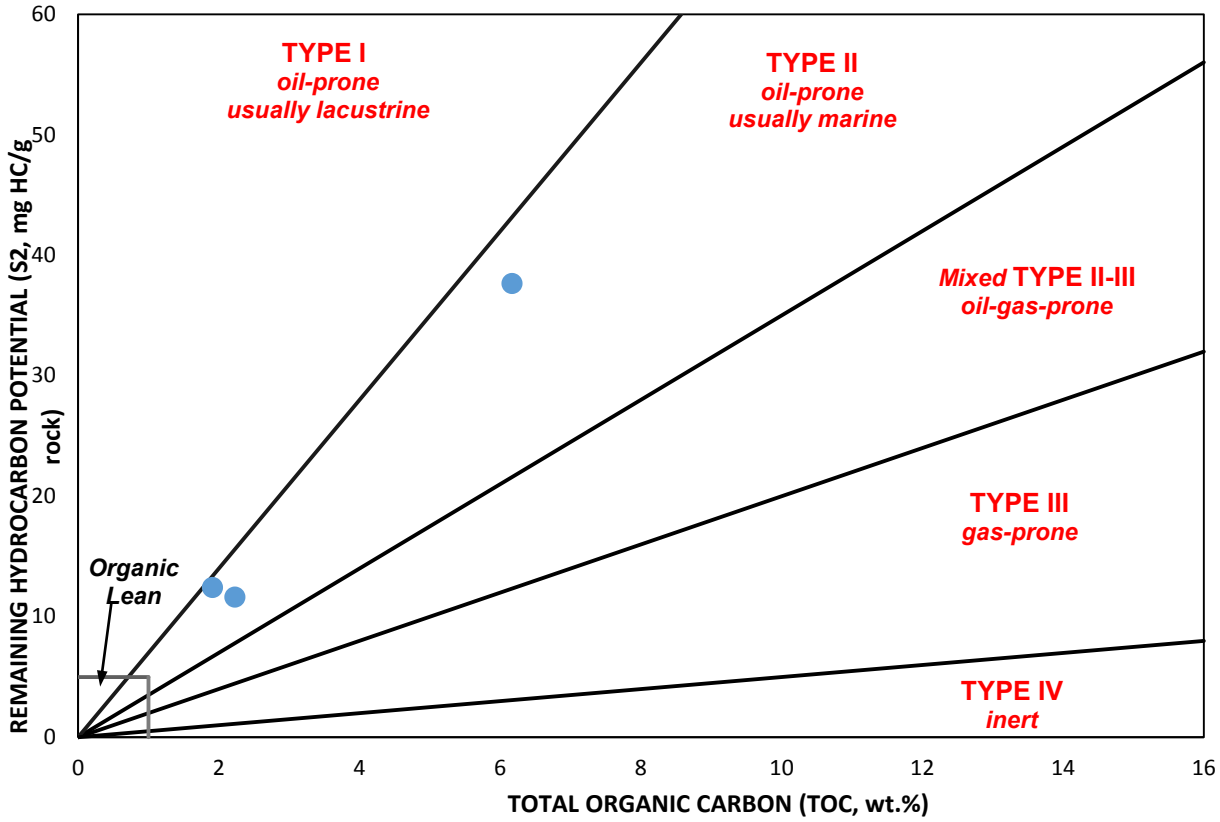

Figure 3.5- Viola Group generative potential (S2) vs. total organic carbon proportion. Note the samples consist of Type II organic matter.

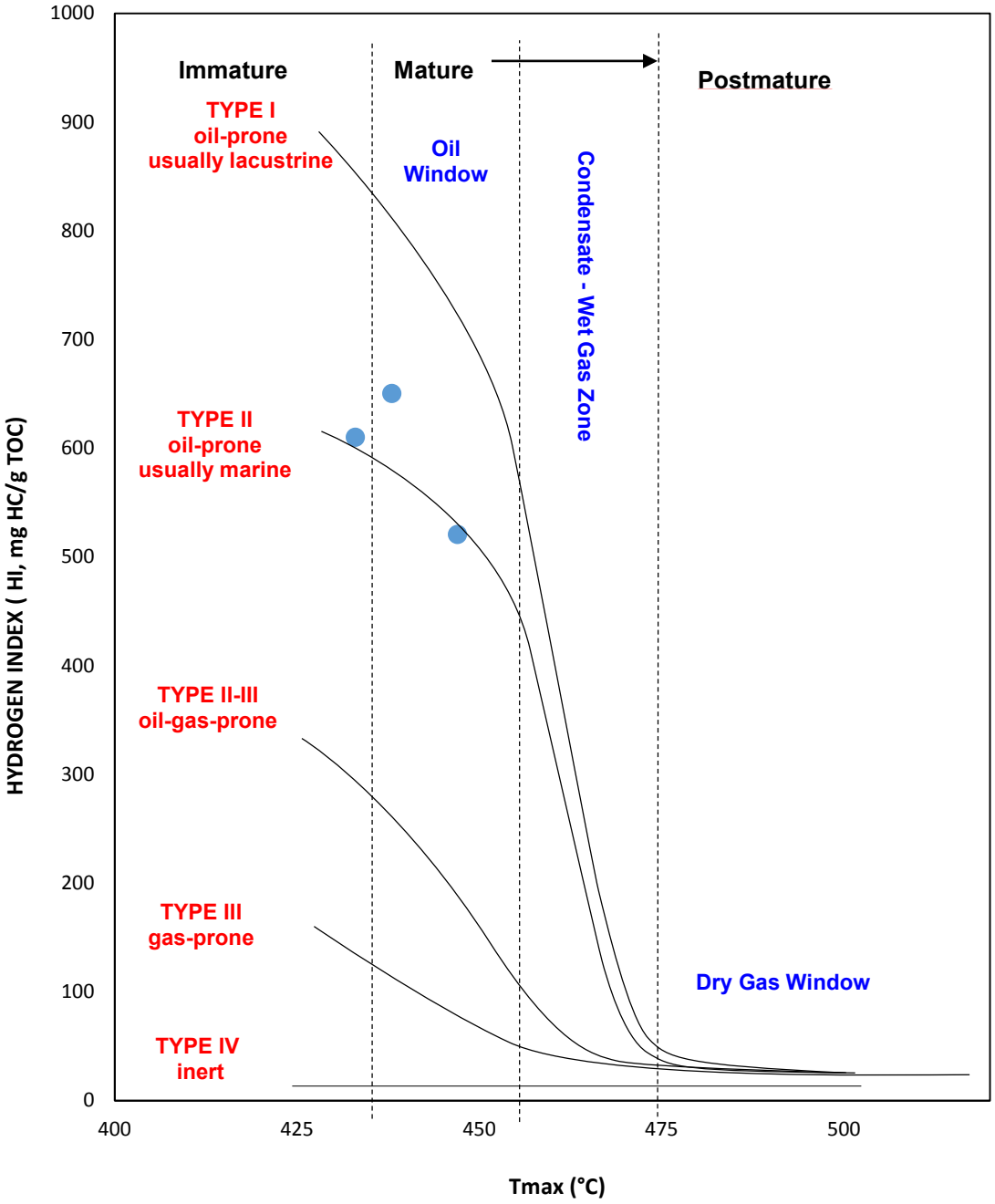

Figure 3.6- Thermal maturity and organic matter type of Viola Group. Data from T_{max} and HI values shows the samples are immature to mature.

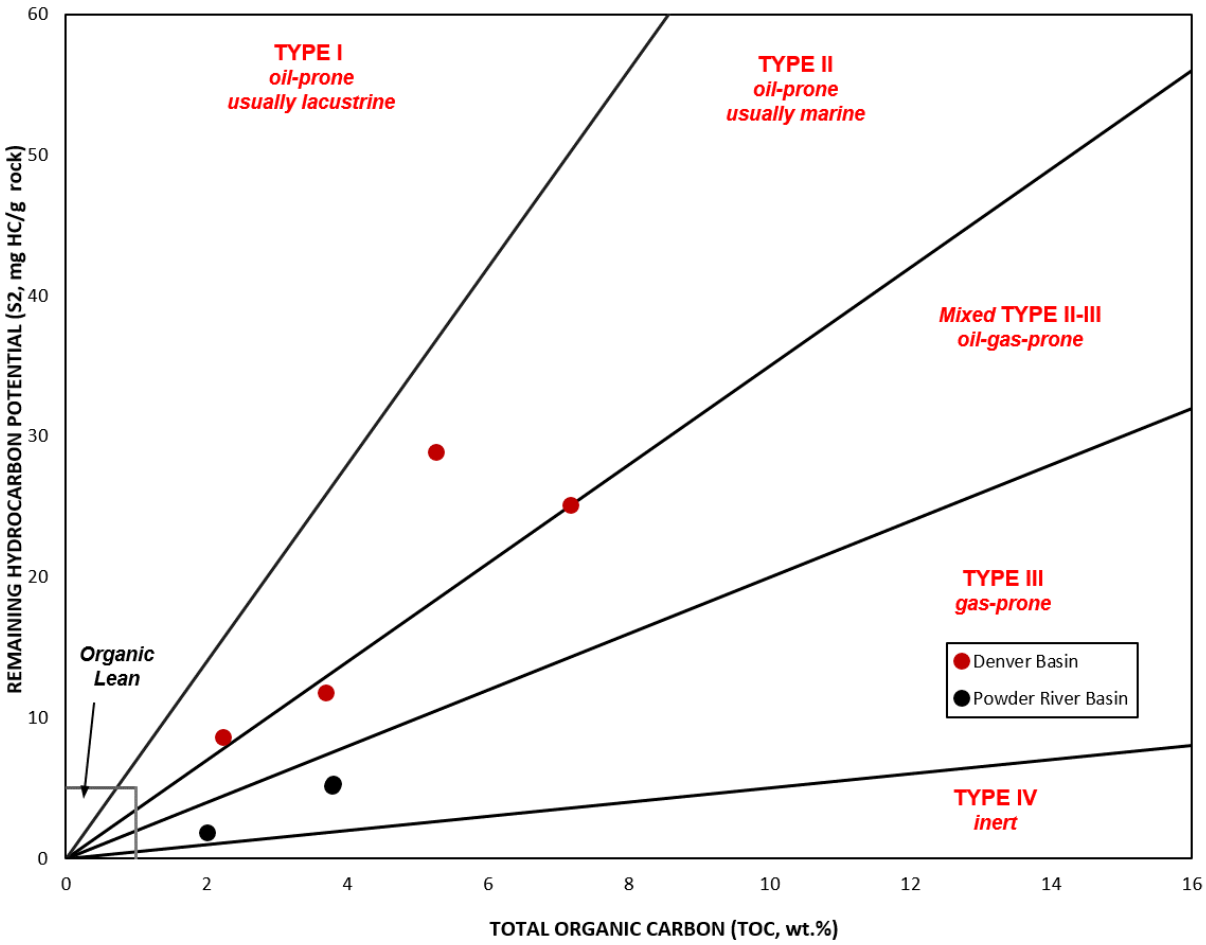

Figure 3.7- Plot of S2 vs. TOC for Niobrara samples showing types of organic matter. Black symbols indicate Powder River Basin samples, red colors indicate Denver Basin samples.

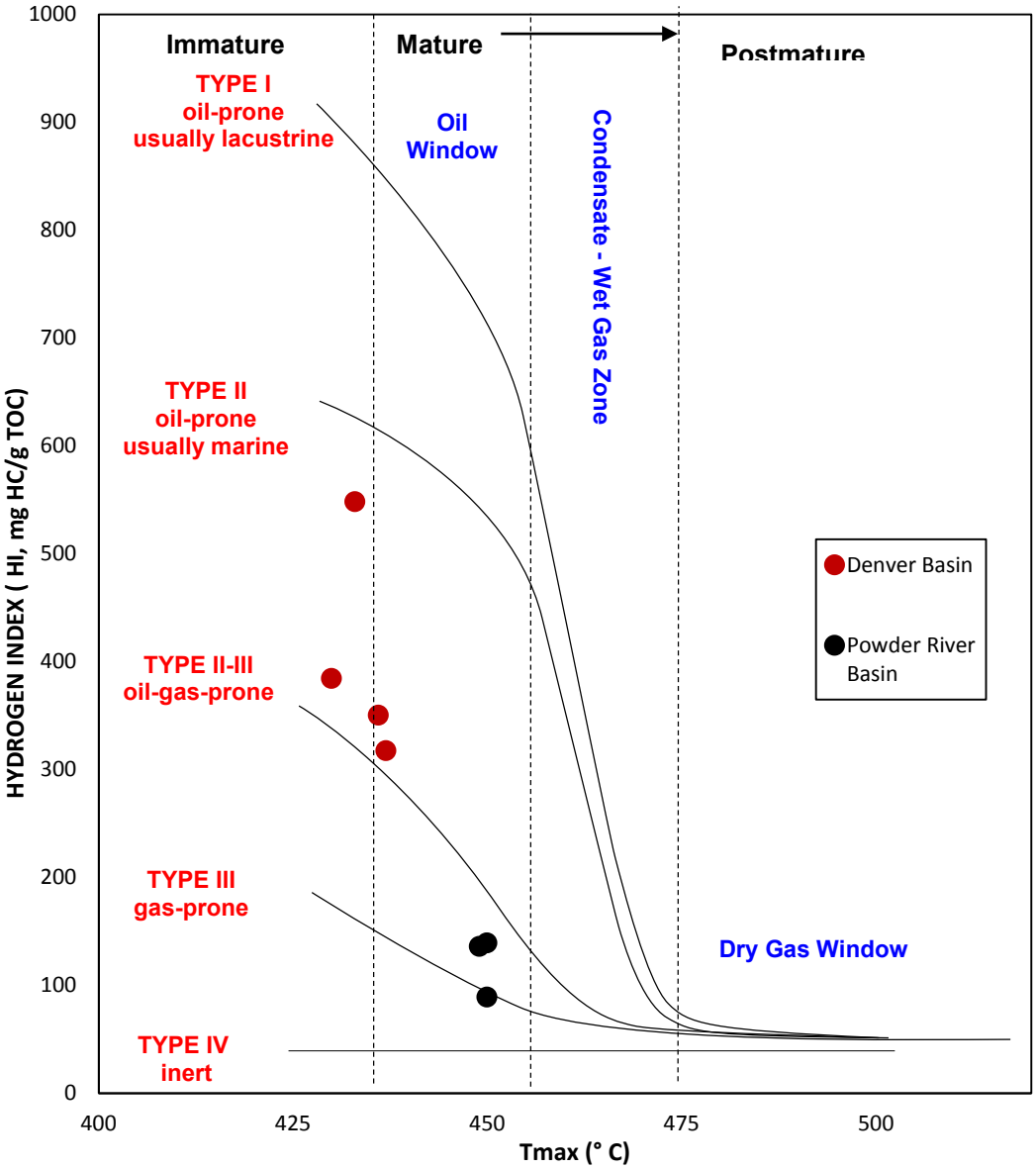

Figure 3.8- Plot comparing HI vs. T_{max} illustrating thermal maturity of Niobrara samples. Samples are immature to mature.

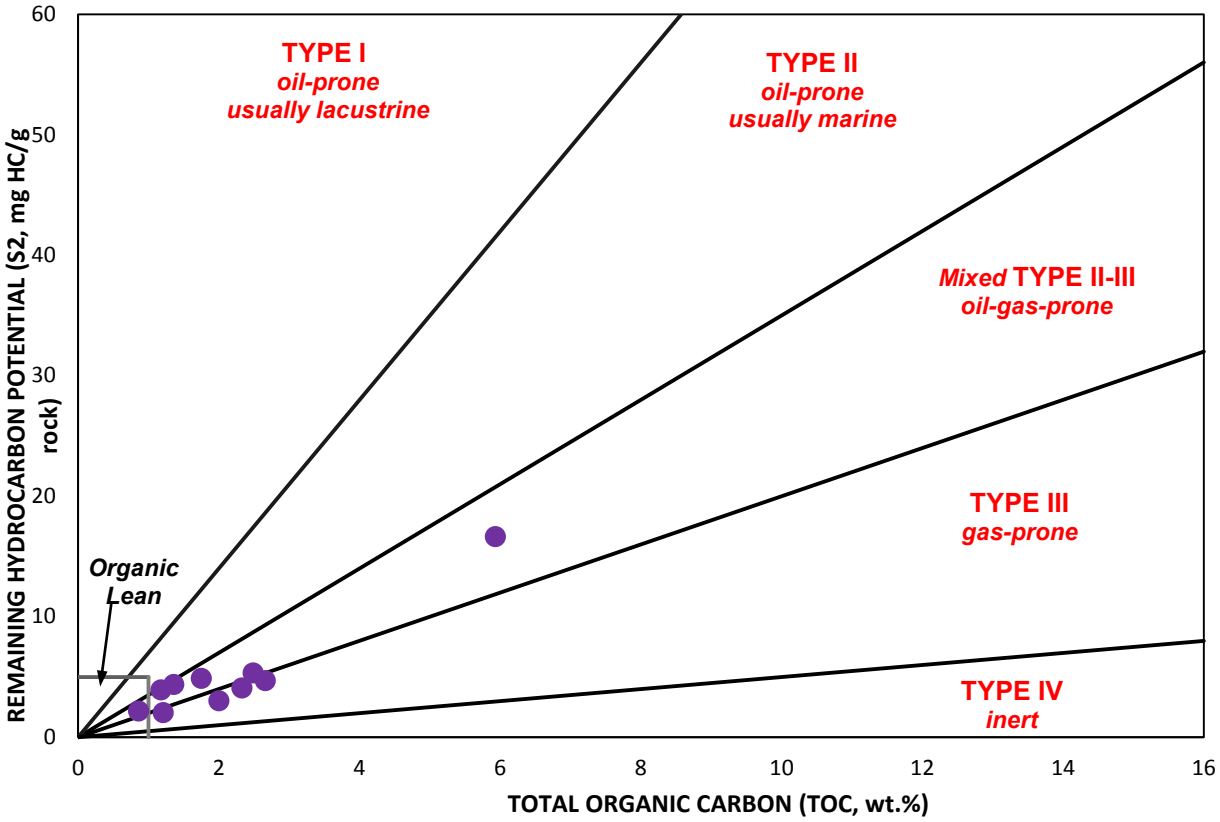

Figure 3.9- Plot of S2 vs. TOC for Silurian "hot shale" samples comparing organic richness and generation potential, showing organic matter type.

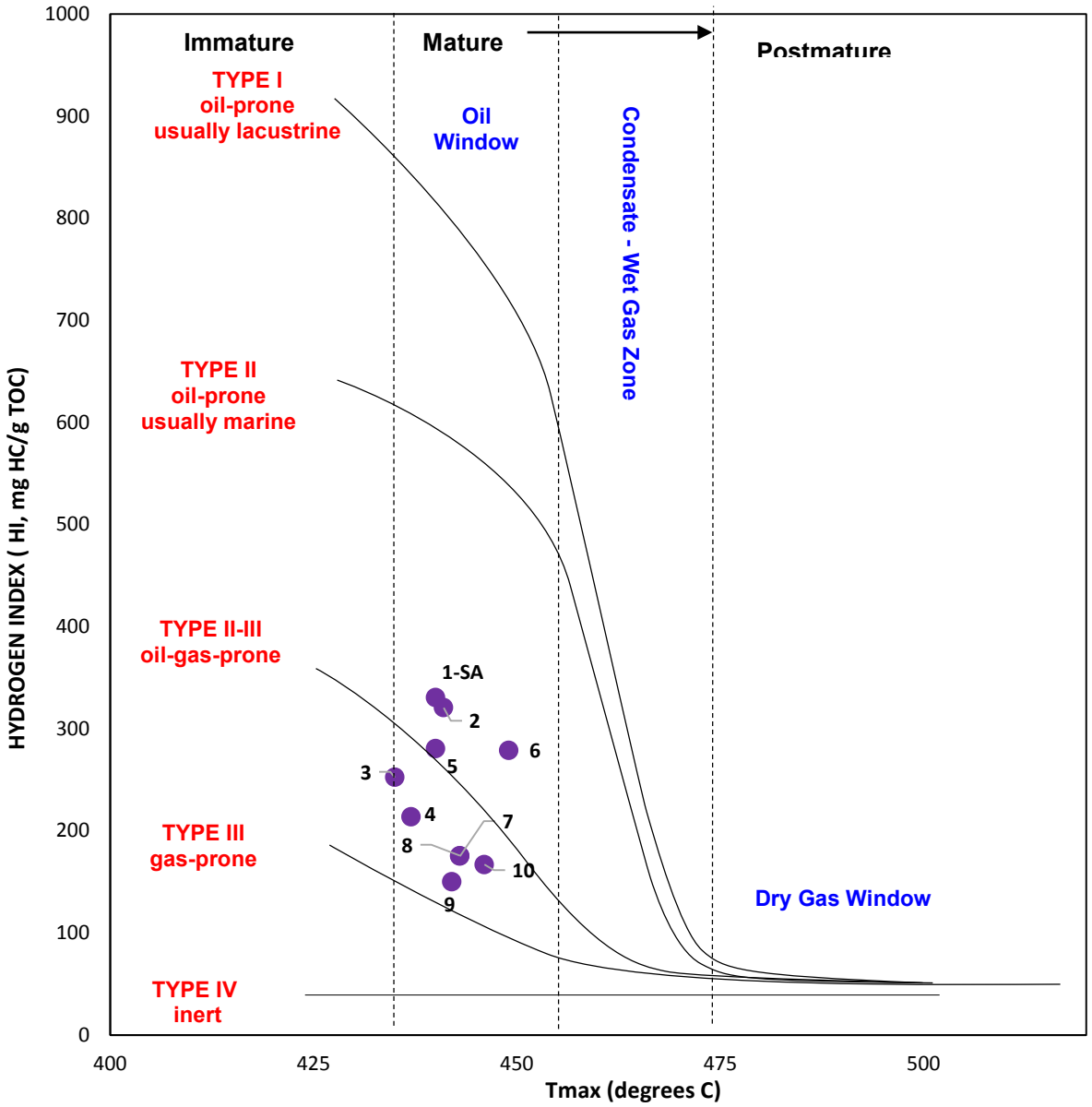

Figure 3.10- Silurian "hot shale" HI vs. T_{max}, notice that samples are mature.

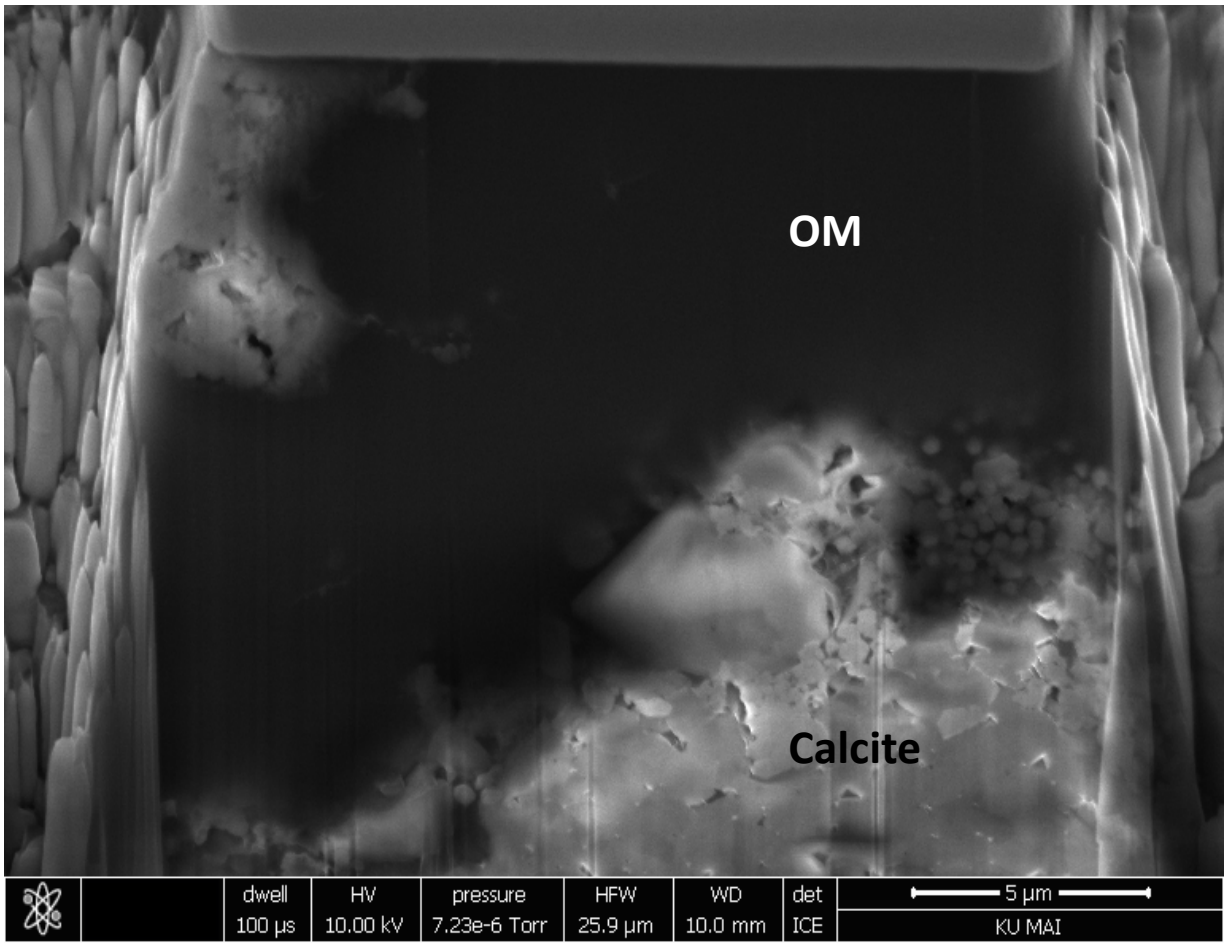

Figure 3.11- Photo of FIB-SEM cross section of sample from Viola Group that intersected lamellar organic matter. Note the absence of organic porosity. Bulk geochemical data for this sample: calc. %Ro- 0.63; TOC- 6.17%; HI- 610 mg HC/g TOC.

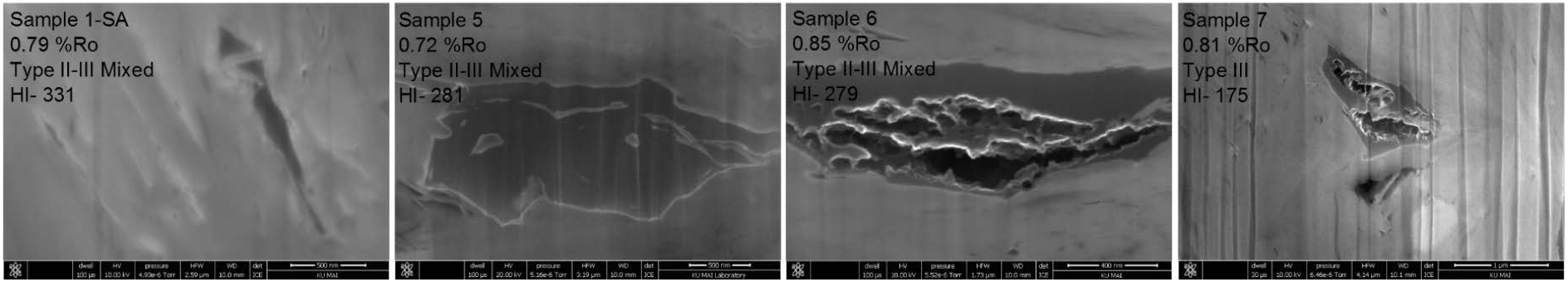

Figure 3.12- Photos of Silurian "hot shale" FIB-SEM cross sections showing increasing organic porosity with decreasing hydrogen index values. Dark gray is organic matter, light gray is calcite matrix, and black "holes" within organic matter are organic pores.

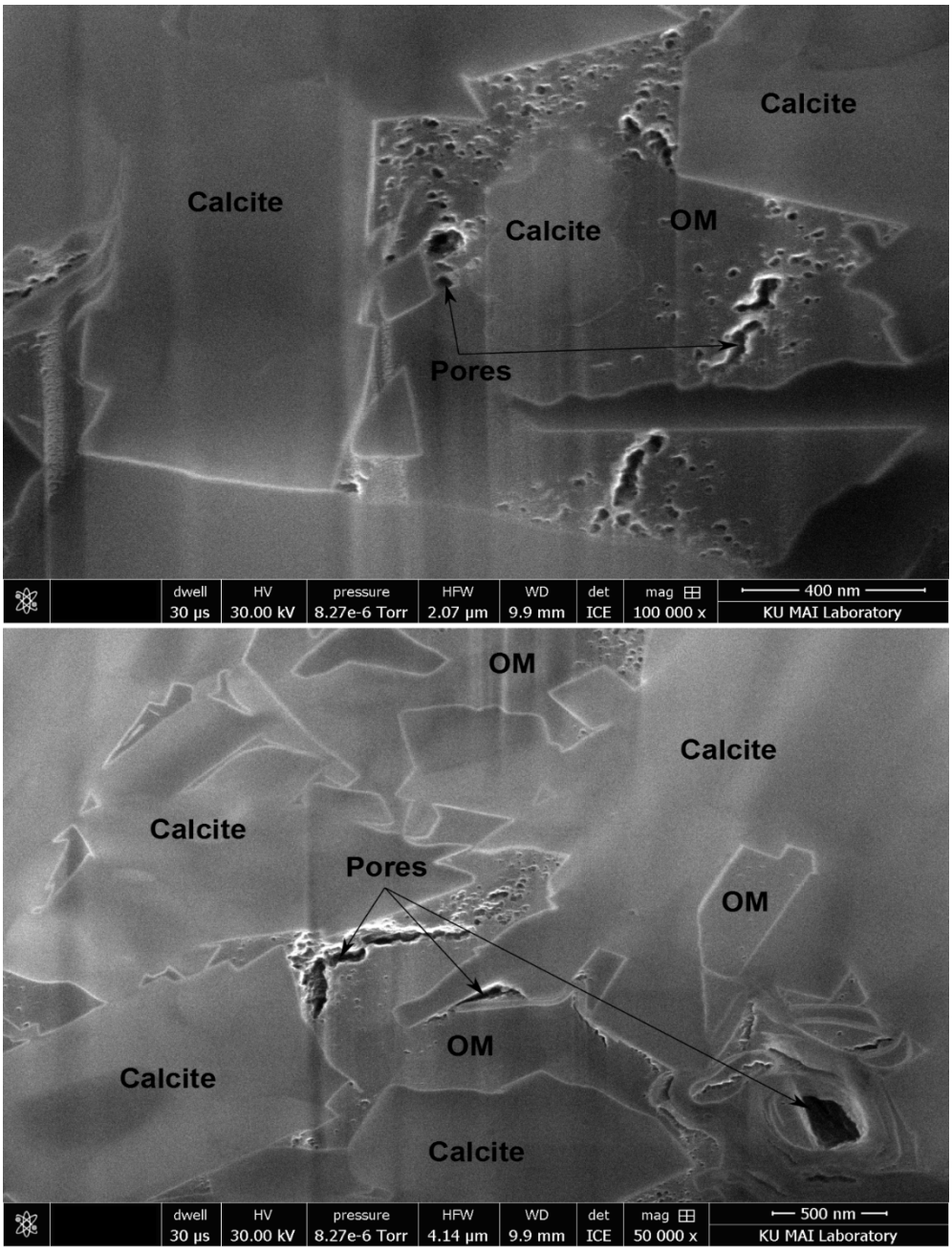

Figure 3.13- FIB-SEM images of Niobrara (sample D779 10390) showing organic porosity. In these images, pores are dark gray to black, organic macerals are gray and matrix is light gray, and the boundaries between organic macerals and calcite matrix are defined by white lines. Note, only some isolated macerals have organic pores, no lamellar OM is present in the sample. Geochemically, this sample is characterized by calc. %Ro- 0.92; TOC- 3.79%; HI- 136 mg HC/g TOC.

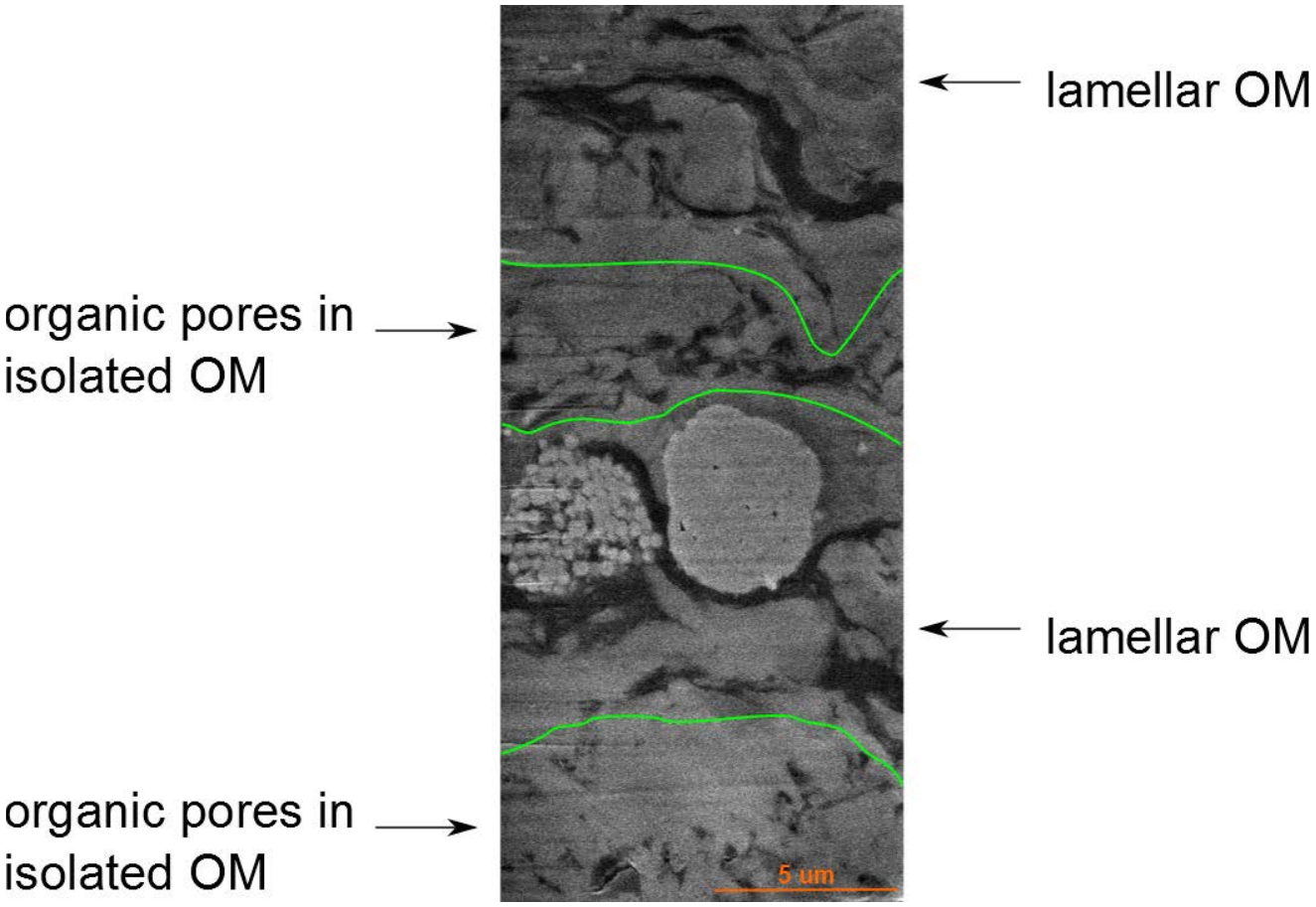

Figure 3.14- Photo of FIB-SEM cross section of Niobrara sample D135 4915. This sample illustrates the microscale variation of organic matter morphology. Organic matter is dark gray to black, matrix and and pyrite framboids are light gray. Layers of lamellar organic macerals are alternating with layers of isolated organic macerals surrounded by matrix. Organic porosity is only evident in isolated organic matter. The green lines represent an inferred transition between the two organic maceral morphologies. Geochemically, this sample is characterized by calc. %Ro- 0.63; TOC- 5.26%; HI- 548 mg HC/g TOC.

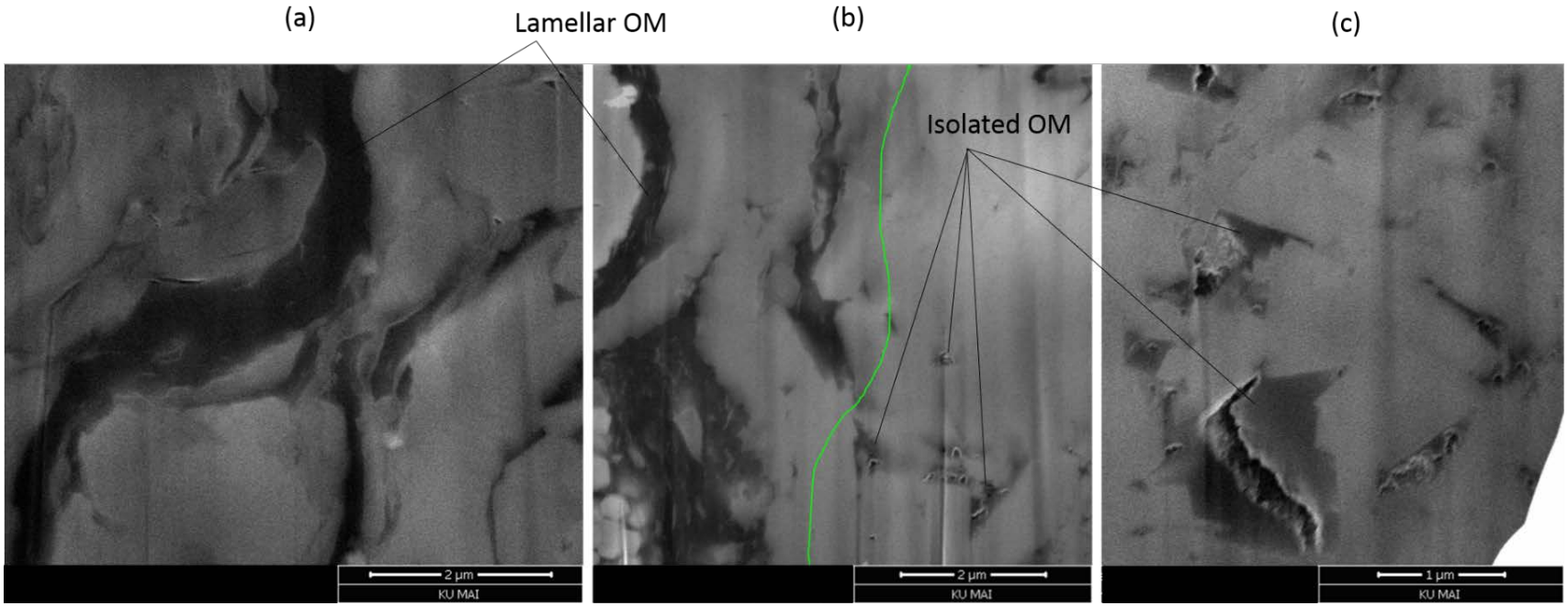

Figure 3.15- Photo of Niobrara FIB-SEM cross sections showing (a) lamellar organic matter (b) lamellar and isolated organic matter. The green line represents an inferred transition between the two organic maceral types (image is rotated, up direction in the core indicated by the arrow) (c) isolated organic matter. Notice the isolated organic macerals contain organic pores, the lamellar organic macerals do not. Geochemically, this sample is characterized by calc. %Ro- 0.63; TOC- 5.26%; HI- 548 mg HC/g TOC.

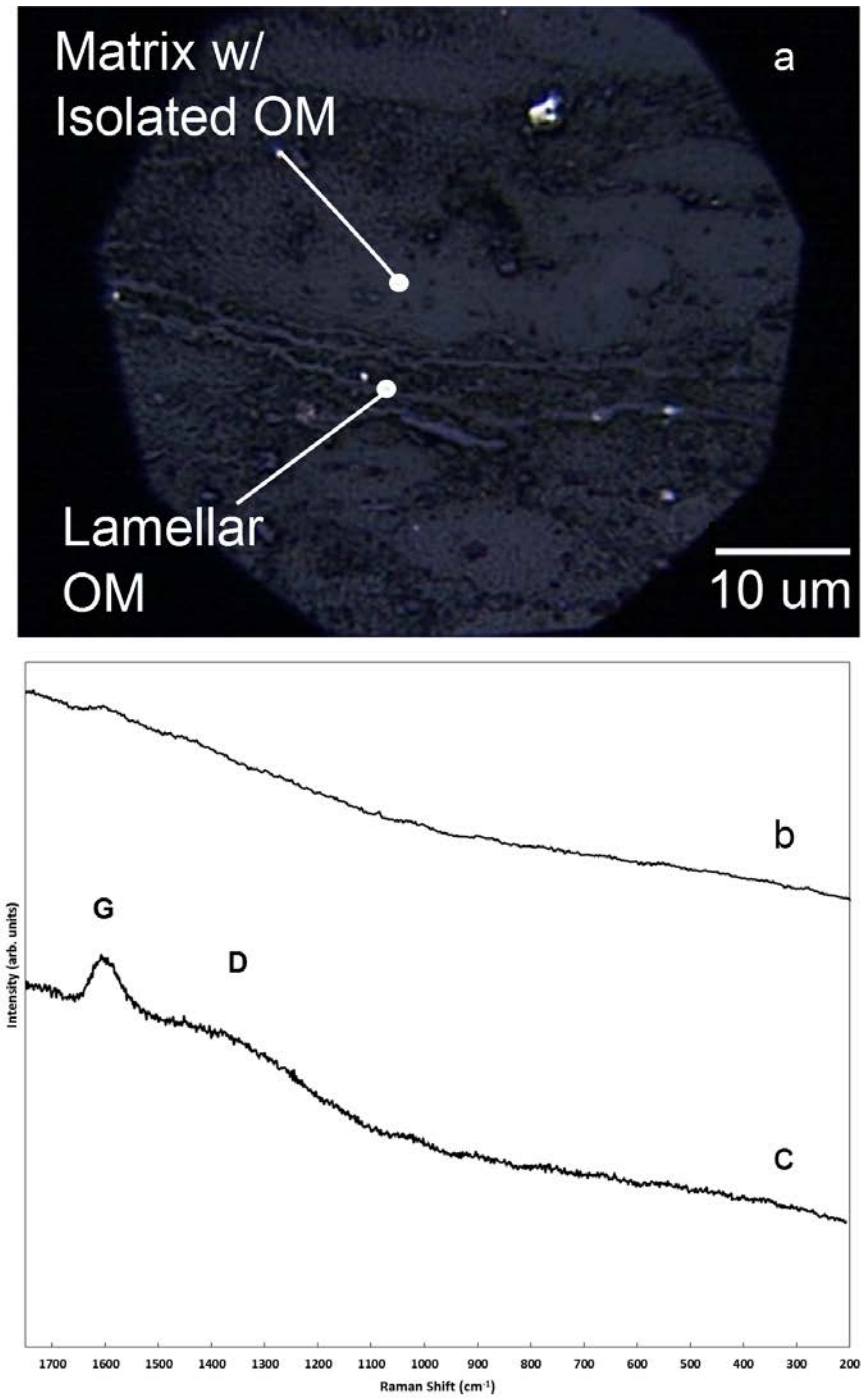

Figure 3.16- Reflected light images of Niobrara sample (D135 4915) showing the locations of Raman spectra collected relative to microfeatures (a). Note that lamellar organic macerals (b) have small and broad G bands, no D band is developed. Isolated organic macerals (c) have more intense and narrow G bands, and a broad D band.

Sample	% porosity
1-SA	0.2
2	1.5
3	1.3
4	1.4
5	1.2
6	2.2
7	1.9
8	2.5
9	1.7
10	1.7

Table 3.1- Silurian "hot shale" Helium pycnometer porosity values. Note, values are < 3% porosity.

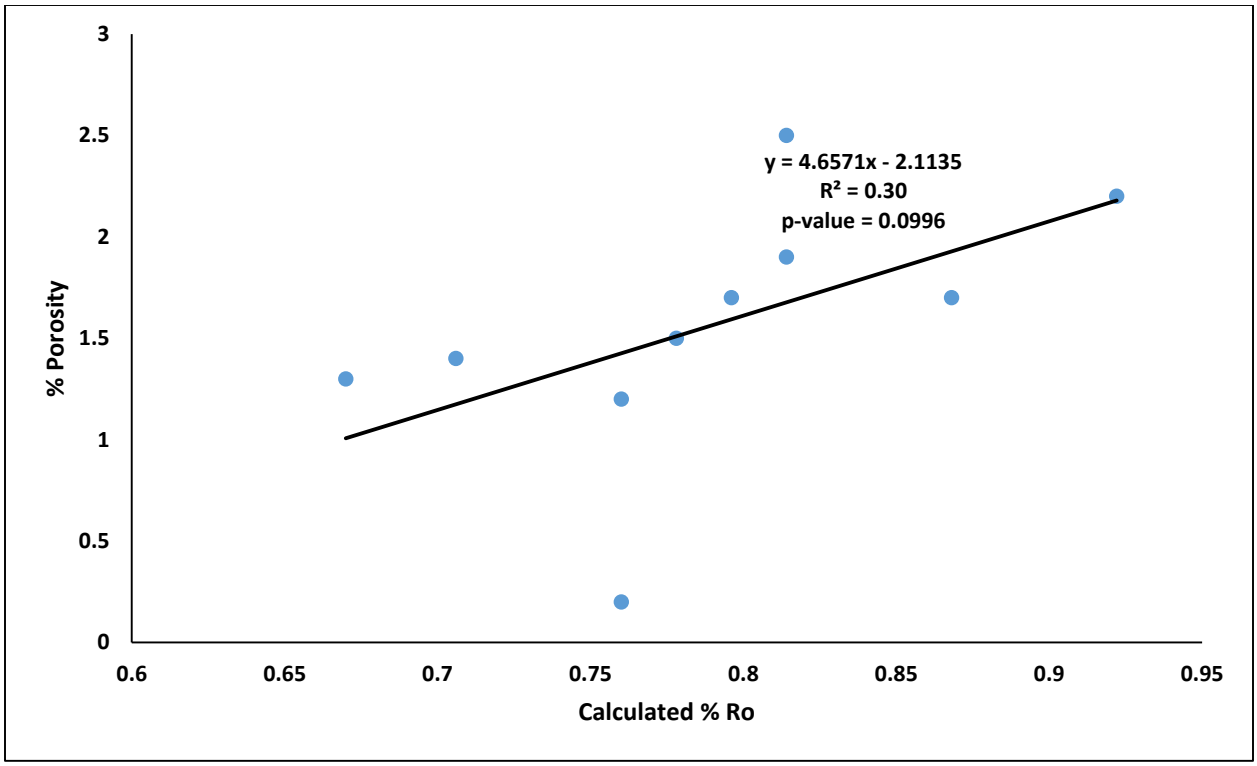

Figure 4.1- Plot of Silurian "hot shale" pycnometer porosity vs. thermal maturity. The data illustrate a positive correlation, $R^2 = 0.30$ is statistically significant at 90% confidence.

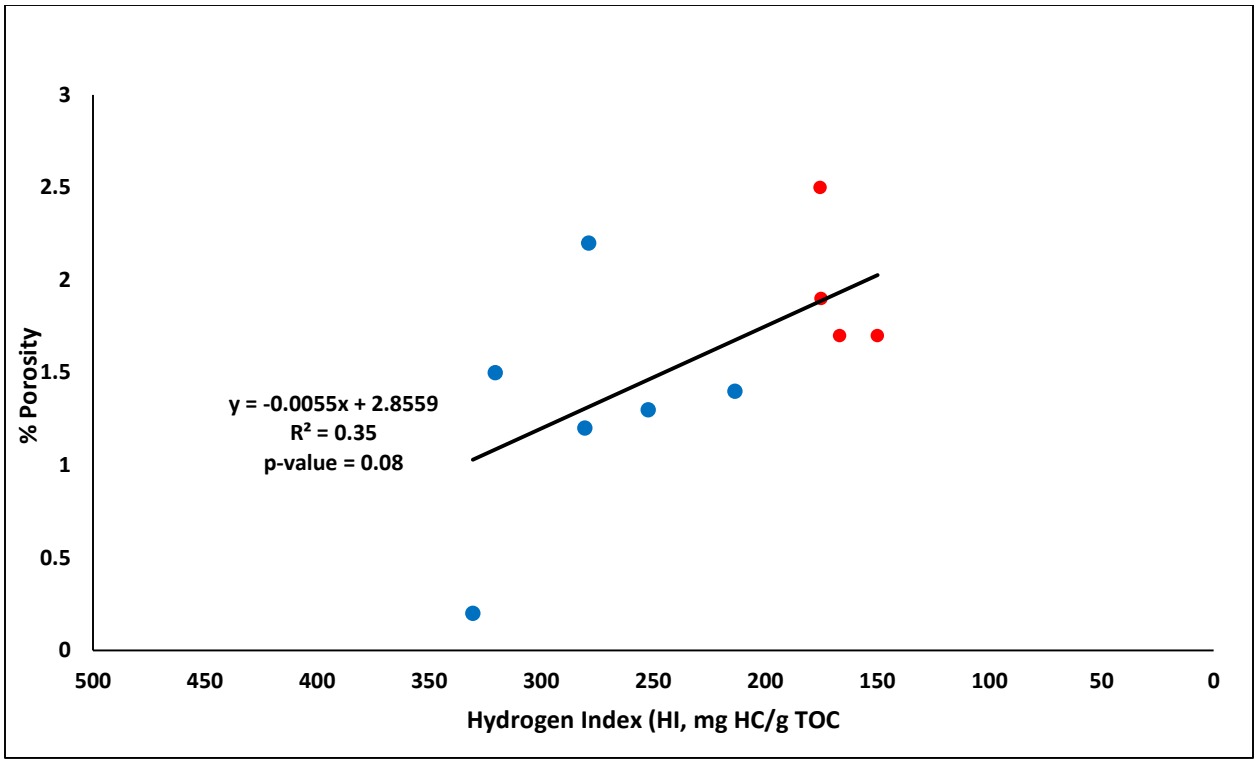

Figure 4.2- Plot of HI values versus porosity. Note the general positive correlation, which is statistically significant at 90% confidence. Type III OM samples (red) have significantly higher porosity (mean = 1.95%) than Type II-III (blue) samples (mean = 1.3%).

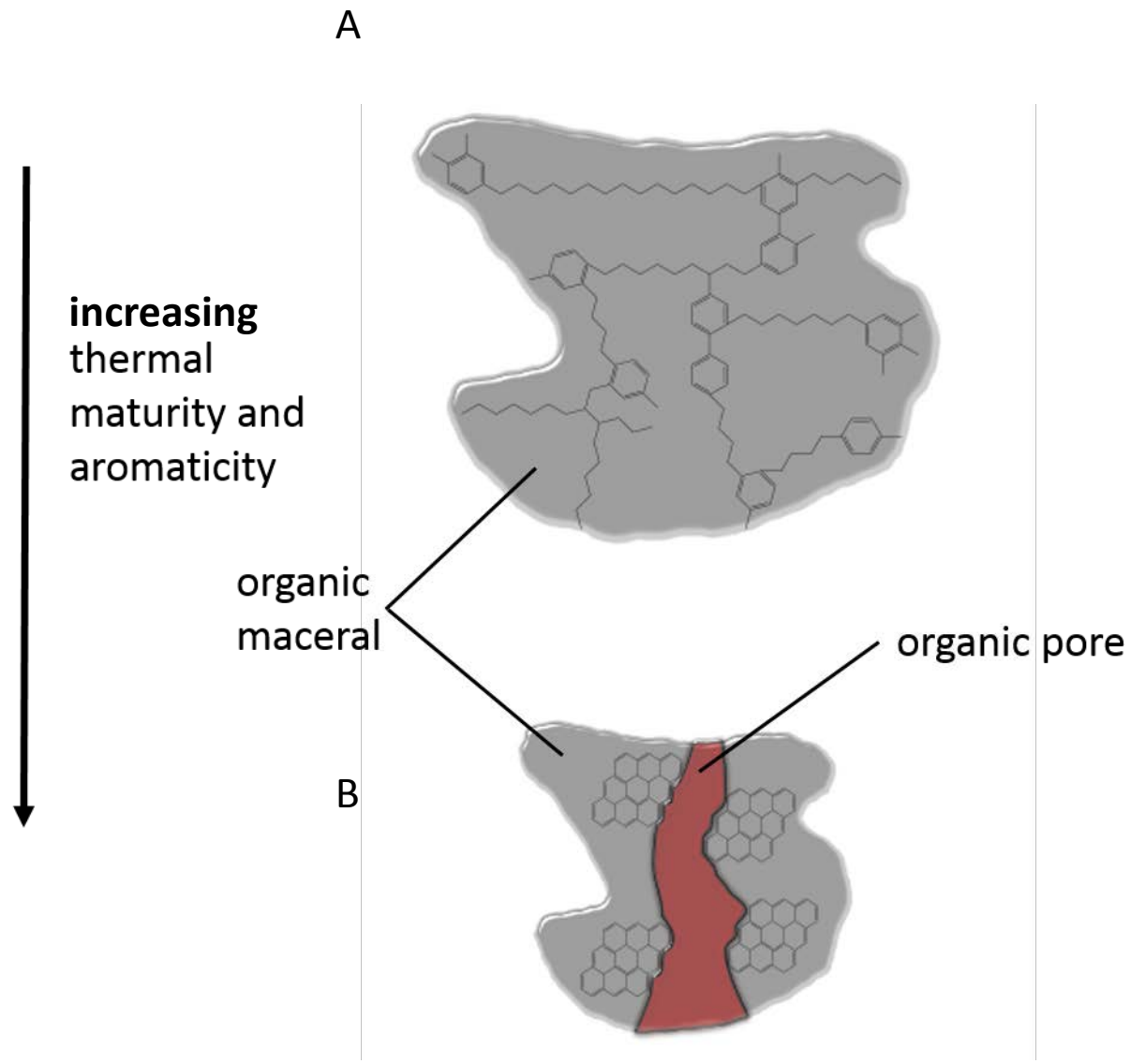

Figure 4.3- Schematic conceptualization showing the influence of increasing thermal maturity on the molecular structure of organic matter, similar to Figure 1.6. (A) Maceral with a highly aliphatic structure and no organic porosity. As thermal maturity increases, the maceral begins to shrink due to de-volatilization reactions (including hydrocarbon expulsion). Aromaticity increases, and the space where volatiles were located become void space (organic pores) resulting in a maceral (B) with aromatic islands surrounded by organic pores. Gray represents organic matter, red represents a crack-like organic pore.

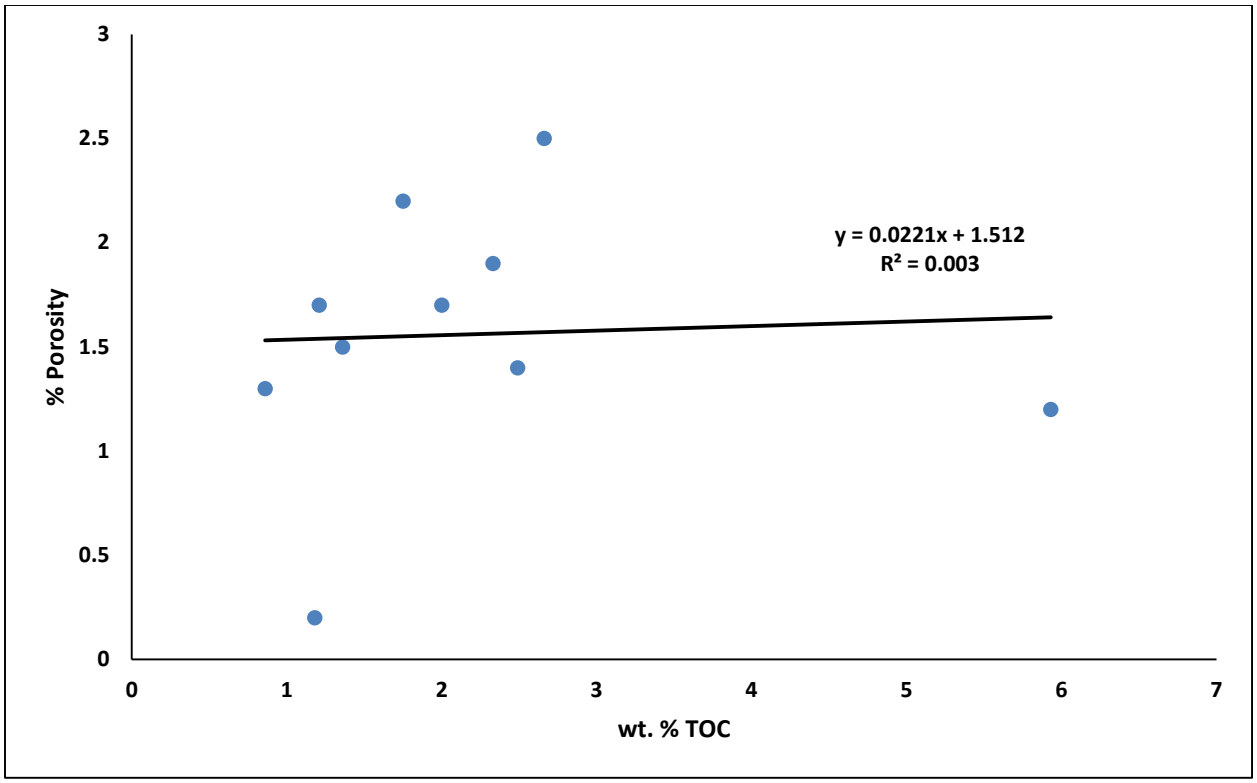

Figure 4.4- Plot of Silurian "hot shale" pycnometer porosity vs. wt. % TOC. Positive covariation exists between TOC and porosity in samples < 5.5 % TOC. No relationship exists between porosity and TOC if all data points are taken into account.